# Exploiting Redundancy to Facilitate Physical Interaction

James Hermus, Johannes Lachner, David Verdi, and Neville Hogan, *Member, IEEE*

***Abstract*—The control of kinematically redundant robots is often approached using nullspace projection, which requires precise models and can be computationally challenging. Humans have many more degrees of freedom than are required to accomplish their tasks, but given neuromechanical limitations, it seems unlikely that biology relies on precise models or complex computation. An alternative biologically inspired approach leverages the compositionality of mechanical impedance. In theory, nullspace projection eliminates any conflict between two tasks. In contrast, superposition of task-space impedance and a full-rank joint-space impedance may impose a task conflict. This work compared nullspace projection with impedance superposition during unconstrained motion and forceful physical interaction. In practice, despite their theoretical differences, we did not observe a substantial influence of the nullspace projector weighting matrix. We found that nullspace projection and impedance superposition both resulted in measurable task conflict. Remarkably, when the dimensionality of the nullspace was increased, impedance superposition was comparable to nullspace projection.**

***Index Terms*—Biological control systems, manipulators, optimal control, robot control.**

## I. Introduction

A PROMINENT challenge in the fields of robotics and human motor control research is to manage systems with a large number of degrees of freedom. Controlling high-degree-of-freedom robots tends to be challenging, especially using popular optimization-based methods, which scale poorly with system dimension. This is the infamous "curse of dimensionality" [1]. Nevertheless, observations from biology are a source of inspiration. Biological systems regularly articulate appendages vastly more complex than state-of-the-art robots and use them to accomplish complex physical interactions such as tool use [2]–[6]. Furthermore, "excess" anatomical degrees of freedom are commonplace in biological systems; the human arm has between 9 and 10 degrees of freedom [7], and the human hand has more than 20 degrees of freedom. It seems peculiar that biology would present this complexity in the configuration of its mechanical structure if it was not complementary to the controller. Perhaps dimensionality is not a "curse" but actually a "blessing," not a "bug" but a "feature." The work reported here explores the notion that a "wealth of degrees of freedom" may alleviate control challenges.

The human arm was one motivation for many of the recently developed seven-degree-of-freedom robotic manipulators (e.g., Kuka LBR iiwa, ABB Yumi - IRB 14 000, Franka Emika, and Rethink Robotics Sawyer). They provide an additional kinematic degree of freedom during the performance of any end-effector task. The work reported in this article investigated approaches to manage this redundancy, not only during free motion but also in tasks, which involve forceful physical interaction. Remarkably, we found that with a sufficient excess of robot degrees of freedom over task degrees of freedom, a superposition of simple impedances performed as well as more complex null-space projection methods.

### A. Managing Redundancy

One way to approach the control of a robot with many degrees of freedom is to express the desired robot behavior in the space of its end-effector actions.[1] This representation is bounded by a maximum number of independent variables ($m \leq 6$). If the differential map $\boldsymbol{J}(\boldsymbol{q}) \in \mathbb{R}^{m \times n}$ (Jacobian) from configuration variables $\boldsymbol{q} \in \mathbb{R}^n$ to end-effector variables is known and the desired end-effector behavior can be expressed as a force $\boldsymbol{f} \in \mathbb{R}^m$, a unique map to joint torques $\boldsymbol{\tau} \in \mathbb{R}^n$ will always exist

$$\boldsymbol{\tau} = \boldsymbol{J}(\boldsymbol{q})^T \boldsymbol{f}. \tag{1}$$

This is a beneficial feature of torque-controlled robots, since (1) also holds for kinematically redundant robots with $n > m$.

Finding the end-effector forces $\boldsymbol{f}$ that are balanced by a given set of joint torques $\boldsymbol{\tau}_f \in \mathbb{R}^n$ represents an optimization problem that may be solved by a generalized inverse of $\boldsymbol{J}(\boldsymbol{q})^T$

$$\boldsymbol{f} = \left(\boldsymbol{J}(\boldsymbol{q})^T\right)^{\#} \boldsymbol{\tau}_f. \tag{2}$$

[1] Also called task space or work space.

Manuscript received February 12, 2021; accepted May 16, 2021. Date of publication July 2, 2021; date of current version February 8, 2022. This work was supported in part by the MechERE Centers at MIT and SUSTech. This paper was recommended for publication by Associate Editor C. Yang and Editor E. Yoshida upon evaluation of the reviewers' comments. *(Corresponding author: James Hermus.)*

James Hermus and David Verdi are with the Department of Mechanical Engineering, Massachusetts Institute of Technology, Cambridge, MA 02139 USA (e-mail: jhermus@mit.edu; dverdi@mit.edu).

Johannes Lachner is with the Department of Electrical Engineering, Mathematics, and Computer Science, University of Twente, Enschede 7522, The Netherlands, and also with the Corporate Research Department, KUKA Deutschland GmbH, Augsburg 86165, Germany (e-mail: j.lachner@utwente.nl).

Neville Hogan is with the Department of Mechanical Engineering, Massachusetts Institute of Technology, Cambridge, MA 02139 USA, and also with the Department of Brain and Cognitive Sciences, Massachusetts Institute of Technology, Cambridge, MA 02139 USA (e-mail: neville@mit.edu).

This article has supplementary material provided by the authors and color versions of one or more figures available at https://doi.org/10.1109/TRO.2021.3086632.

Digital Object Identifier 10.1109/TRO.2021.3086632

1552-3098 © 2021 IEEE. Personal use is permitted, but republication/redistribution requires IEEE permission.
See https://www.ieee.org/publications/rights/index.html for more information.

Authorized licensed use limited to: MIT Libraries. Downloaded on February 09,2022 at 17:31:09 UTC from IEEE Xplore. Restrictions apply.

If $n > m$, a nullspace exists in $(\boldsymbol{J}(\boldsymbol{q})^T)^{\#} \in \mathbb{R}^{m\times n}$. This means that the end-effector forces can be balanced with infinitely many different joint torque solutions. The kernel of the optimization is the weighting matrix $\boldsymbol{W} \in \mathbb{R}^{n\times n}$

$$\boldsymbol{J}(\boldsymbol{q})^{\#} = \boldsymbol{W}^{-1}\boldsymbol{J}(\boldsymbol{q})^T\left(\boldsymbol{J}(\boldsymbol{q})\boldsymbol{W}^{-1}\boldsymbol{J}(\boldsymbol{q})^T\right)^{-1}. \tag{3}$$

Accordingly, $\boldsymbol{J}(\boldsymbol{q})^{\#}$ yields a joint torque that minimizes the quadratic cost

$$g(\dot{\boldsymbol{q}}) = \frac{1}{2}\dot{\boldsymbol{q}}^T\boldsymbol{W}\dot{\boldsymbol{q}}. \tag{4}$$

The projector in the nullspace of $(\boldsymbol{J}(\boldsymbol{q})^T)^{\#}$ can be expressed by

$$\boldsymbol{N}_\tau = \boldsymbol{I} - \boldsymbol{J}(\boldsymbol{q})^T\left(\boldsymbol{J}(\boldsymbol{q})^T\right)^{\#} \tag{5}$$

where $\boldsymbol{N}_\tau \in \mathbb{R}^{n\times n}$. All torques $\boldsymbol{\tau}_{\text{any}} \in \mathbb{R}^n$ that are projected into this nullspace do not interfere with end-effector forces of higher priority and can be used for additional tasks [8]–[11], e.g., to avoid obstacles or joint limits

$$\boldsymbol{\tau} = \boldsymbol{J}(\boldsymbol{q})^T\boldsymbol{f} + \boldsymbol{N}_\tau\boldsymbol{\tau}_{\text{any}}. \tag{6}$$

Note that $\boldsymbol{\tau}_{\text{any}}$ can incorporate further projections in the nullspace of lower priority tasks. In this way, arbitrarily many task levels can be produced with either the successive [9] or augmented [11], [12] methods. The lowest priority level is often chosen to be a joint damper to avoid oscillations due to nullspace motions [13]. The feasibility of these task levels depends on the dimension of the nullspace, i.e., a 1-D nullspace only allows projection of a 1-D task. Hence, theoretically, a robot with $n >> m$ degrees of freedom is capable of accomplishing multiple tasks, without disturbing the main task.

The literature on redundancy resolution is predominantly concerned with nullspace projection approaches [12], [14]–[21]. A general overview of nullspace projections was presented in [22]. Implementations of hierarchical nullspace-projection-based control have been applied to tasks which involve contact [9], [11], [23]–[29] and systems with multiple contact points [10], [30], [31]. Problems with instabilities have been discussed in [32] and [33]. This led to the development of conservative nullspace projection methods [34], [35]. Stable nullspace projection methods have also been developed for mobile robot platforms [8], [36]–[38] and to cope with velocity actuator saturation [39]. Energy tank methods have been applied to render nullspace projection methods passive [40], [41].

*1) Mechanical Impedance Superposition:* While many approaches have been developed to ensure stability when nullspace projections are employed, neither the nullspace projector nor the stabilizing corrections would be required if each controller were formulated as an energetically passive impedance. A simple—even naive—solution to control the desired dynamic robot behavior can be achieved by assigning a set of impedances, which can be visualized as a spring-damper system [42]–[45]. These impedances can be applied in end-effector space and in joint-space. Even if these impedances are nonlinear, they can be superimposed

$$\boldsymbol{\tau} = \sum_{i=1}^{k}\boldsymbol{J}(\boldsymbol{q})_i^{\boldsymbol{T}}\; Z\{\boldsymbol{x}\}_i + \sum_{j=1}^{l} Z\{\boldsymbol{q}\}_j \tag{7}$$

with $k$ end-effector impedances $Z\{\boldsymbol{x}\}_i : \mathbb{R}^m \to \mathbb{R}^m$ and $l$ joint impedances $Z\{\boldsymbol{q}\}_j : \mathbb{R}^n \to \mathbb{R}^n$. If each component impedance is passive, their sum is energetically passive, and since no inverse kinematics are needed, this approach works at kinematic singularities.

If $n > m$, the end-effector impedance does not control the nullspace of $\boldsymbol{J}(\boldsymbol{q})$. To achieve predictable joint motion, a full-rank set of joint-space impedances can be assigned. These impedances push the robot toward a desired configuration $\boldsymbol{q}_0$. However, the joint-space impedance may conflict with the end-effector impedance—which is usually the task of interest—except in the rare cases when the end-effector position corresponds to that configuration $\boldsymbol{q}_0$. This may be the reason why nullspace projection approaches have rarely [46] been compared with impedance superposition: in theory nullspace projection approaches should eliminate the end-effector task error, while the simple superposition of impedance controllers may result in task conflict. However, as we show below, due to imperfections in a robot's kinematic and dynamic models, in practice nullspace projection may also cause task-space disruption.

One novel aspect of the work reported here is that it assessed task-space errors due to implementing both approaches on hardware. For nullspace projections, we assigned different weighting matrices. The choice of nullspace weighting matrix has been discussed in several contexts: to generate favorable kinematic behavior [47], prioritize different motions [48], perform motion control with joint constraints [49], [50], and ensure dynamic consistency [13]. In this work, we compare nullspace projection methods to the superposition of mechanical impedance in both unconstrained motion and during physical interaction with a constraint.

### B. Factors That Influence Controller Design

To find an appropriate control approach for a given robot task, many factors should be considered. Some factors are determined by the robotic system and the environment with which it interacts. Another factor is the available information about the robot model, i.e., kinematic and/or dynamic data. Finally, the desired task may or may not be achievable by the robot. We took several of these factors into account when comparing nullspace projection methods with impedance superposition.

*1) Environmental Factors:* A robot is influenced by its own controller and the dynamics of the environment which acts on it. Since it is impossible to have a perfect model (or in many cases even a competent model) of the interacting environment [51], most algorithms solely concentrate on the robot's controller. With an impedance controller, a desired interactive dynamic behavior can be implemented (though perhaps imperfectly). To specify how well a robot performs its tasks both in and out of contact, quantitative measures are required. In unconstrained motion, we assessed the difference between the desired and actual position and orientation. In tasks involving continuous

Authorized licensed use limited to: MIT Libraries. Downloaded on February 09,2022 at 17:31:09 UTC from IEEE Xplore. Restrictions apply.

TABLE I
OPTIMIZATION CRITERIA FOR NULLSPACE PROJECTORS

| Weighting matrix | Cost | Description |
|---|---|---|
| $\boldsymbol{W}^{-1} = \mathbf{0}$ | – | Impedance Superposition |
| $\boldsymbol{W} = \boldsymbol{I}$ | $\frac{1}{2}\dot{\boldsymbol{q}}^T\dot{\boldsymbol{q}}$ | Least Velocity Norm |
| $\boldsymbol{W} = \boldsymbol{M}(\boldsymbol{q})$ | $\frac{1}{2}\dot{\boldsymbol{q}}^T\boldsymbol{M}(\boldsymbol{q})\dot{\boldsymbol{q}}$ | Least Kinetic Energy |
| $\boldsymbol{W} = \boldsymbol{B}_q$ | $\frac{1}{2}\dot{\boldsymbol{q}}^T\boldsymbol{B}_q\dot{\boldsymbol{q}}$ | Least Energy Dissipation |
| $\boldsymbol{W} = \boldsymbol{K}_q$ | $\frac{1}{2}\Delta\boldsymbol{q}^T\boldsymbol{K}_q\Delta\boldsymbol{q}$ | Least Potential Energy |

physical interaction, the deviations between desired and actual forces were used as a quantitative measure of controller performance.

*2) Nullspace Dimension:* Most industrial robots are serial kinematic chains with six degrees of freedom. Since it is desirable to describe the robot task in end-effector space, these robots have the benefit that the mapping between end-effector space and joint-space is bijective. However, in practice many tasks require fewer degrees of freedom. For example, consider a robot with a welding gun: rotation of the gun about its long axis has no influence on task performance. Thus, even a six-degree-of-freedom robot is redundant with respect to some tasks. Of course, serial kinematic chain robots with seven degrees of freedom or more always exhibit a nullspace, but the dimension of the nullspace depends on the end-effector task. Nullspace projection methods can take advantage of redundancy by assigning additional tasks in the nullspace of the main task. In the work reported here, we investigated whether there could be advantages to decreasing the task dimensions and thereby increasing the nullspace dimensions.

*3) Weighting Matrix:* Nullspace projection methods require a weighting matrix. This weighting matrix defines the cost function minimized in the optimization, as seen in (4). Even though any positive definite matrix can be used, without a meaningful choice, physical insight may be lost [52]. A list of some possible options can be seen in Table I. Two common choices are $\boldsymbol{W} = \boldsymbol{I}$ and $\boldsymbol{W} = \boldsymbol{M}(\boldsymbol{q})$. The former yields the least-norm solution [53] and the latter minimizes the kinetic energy [13], [54] produced by nullspace motion. The dynamic consistency provided by the mass matrix is superior [22], [55] especially when inertial dynamics are significant. In theory, this is the only nullspace projector that does not produce accelerations that interfere with the main task. Moreover, it is the only projector that does not inject energy during nullspace motion and should therefore have superior stability properties [54]. However, in practice, without a perfect model of the mass matrix, other choices may be better [18], [21], [22], [56]. Often when working with low-cost robots, the mass matrix is not well known. In addition, poorly modeled joint friction and motor rotational inertia, amplified through a gear transmission, may dominate the dynamic response of the robot [57]. Yet another reasonable choice is $\boldsymbol{W} = \boldsymbol{B_q}$. By using the joint-space damping matrix $\boldsymbol{B_q} \in \mathbb{R}^{n\times n}$, the nullspace motion with least energy dissipation is produced. The choice $\boldsymbol{W} = \boldsymbol{K_q}$ produces the solution that minimizes potential energy at equilibrium. We acknowledge that there are many other weighting matrix choices not considered here, including [47]–[50]. For notational convenience, we also define $\boldsymbol{W}^{-1} = \mathbf{0} \in \mathbb{R}^{n\times n}$, a matrix with only zero entries. With this, the nullspace projection matrix is equal to the identity matrix, corresponding to a superposition of all task levels.

*4) Inertial Dynamics:* A robot's performance is affected by its inertial dynamics. If the robot moves slowly enough, inertial dynamics can be neglected and the task can be considered quasi-static. At fast speeds, however, inertial dynamics, damping, and stiffness must all be considered. The choice of task execution speed (slow/quasi-static versus fast/dynamic) was expected to have a substantial impact on task performance for certain choices of nullspace projection weighting matrices.

*5) Relative Impedance Magnitudes:* Using impedance superposition, a large joint-space impedance will result in a substantial conflict with any end-effector task, while a smaller joint-space impedance will evoke a lesser conflict. This prompted the question: if a small joint-space impedance, sufficient to "manage the redundancy"[2] is superimposed, how large will the task disruption be? When comparing mechanical impedance superposition and nullspace projection methods, the magnitude of the joint-space stiffness was taken into account.

### C. Summary

The principal aim of this study was to quantify and compare the performance of mechanical impedance superposition and nullspace projection methods to manage redundancy on real hardware in practice. Quantitative assessment was performed during both unconstrained and constrained motion. A secondary aim was to understand and quantify how the dimension of the nullspace—the wealth of degrees of freedom—influenced performance. Our results show that for a nullspace of sufficient dimension, the task conflict from simple impedance superposition was comparable to that of all nullspace projection methods.

## II. METHODS

The goal of these experiments was to examine the behavior of a redundant robot placed under an end-effector impedance controller (Task 1), along with a joint-space impedance controller (Task 2). Task 2 was either superimposed directly ($\boldsymbol{W}^{-1} = \mathbf{0}$) or projected into the nullspace of Task 1 using each of the four weighting matrices listed in Table I. The experiments investigated both unconstrained motion and forceful physical contact with a circular constraint, specified in Task 1. For all five weighting matrices, performance was quantified for different nullspace dimensions, joint stiffnesses, and task speeds.

[2]This was defined operationally as an impedance as small as possible, but still capable of restoring the robot to a position near its nominal configuration after a large null-space position disturbance.

Authorized licensed use limited to: MIT Libraries. Downloaded on February 09,2022 at 17:31:09 UTC from IEEE Xplore. Restrictions apply.

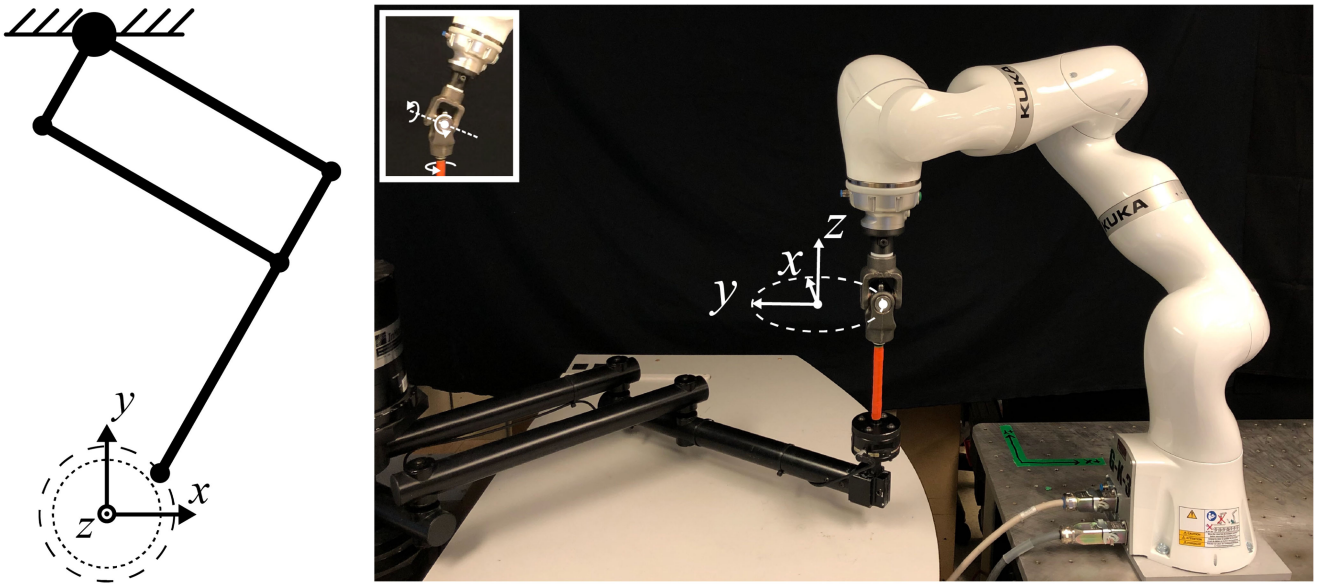


Fig. 1. Experimental setup. (Left) Planar depiction of the InMotion Robot and reference frame. The dotted circle denotes the zero-force trajectory of the InMotion robot and the dashed circle denotes the zero-force trajectory of the LBR. (Right) The LBR was coupled with a U-joint and sleeve bearing to the handle of the InMotion robot. The inset in the upper left illustrates the rotational degrees of freedom allowed by the U-joint and sleeve bearing.

### A. Experimental Setup

All experiments were conducted with a seven degree of freedom torque-controlled KUKA LBR iiwa R800 (LBR) [58]. To facilitate measurement, in each experiment the LBR was coupled to a customized InMotion2 Shoulder-Elbow robot (Interactive Motion Technologies Inc.) via a U-joint and bearing connection. The InMotion is a highly back-drivable light-weight torque controlled $x-y$ planar robot, which was designed for stroke rehabilitation and human motion research. The custom control system for the InMotion robot was implemented on a CompactRIO 9034 controller, with low-level functionality implemented at 2 kHz on a CompactRIO FPGA, and high-level functionality implemented at 1 kHz on a CompactRIO real-time processor. InMotion joint positions were measured by a 16-bit/rev encoder and interaction forces were measured at the end-effector of the InMotion robot using an ATI Gamma force/torque transducer [59], [60]. The experimentally coupled robots are shown in Fig. 1.

The U-joint (Neapco Components, Pottstown, PA) and bearing connection enabled a $\pm 45^{\circ}$ rotational range of motion about the $x$ and $y$ axes. Rotation around the $z$-axis was facilitated by an ultra-low-friction dry-running sleeve bearing, which also enabled translation along the $z$-axis. Thus, if the center of the U-joint is viewed as the kinematic coupling point, the two robots are constrained relative to each other translationally in the $x-y$ plane, but not constrained translationally along the $z$-axis. Furthermore, the U-joint decoupled rotations about all three axes.

Once the two robots were coupled together with the U-joint and bearing system, the total amount of free-play or backlash in the coupling connection was quantified. The brakes were applied on the LBR, nominally fixing it rigidly in space. The handle of the InMotion robot was then lightly perturbed by hand in several directions, and the resulting handle displacements were measured using the InMotion encoders. It was found that the InMotion handle could undergo a displacement of $\pm 1.5$ mm in the $x-y$ plane without applying appreciable forces to the LBR.

### B. Impedance Controller

The end-effector and joint-space impedance controllers were implemented on the LBR using the KUKA Fast Research Interface (FRI), via an external PC, with torque commands computed at 200 Hz. The FRI friction and gravity compensation was active throughout all of the experiments. The analytical Jacobian matrix $\boldsymbol{J}(\boldsymbol{q}) \in \mathbb{R}^{6\times n}$ of the robot was denoted by

$$\boldsymbol{J}(\boldsymbol{q}) = \begin{bmatrix} \boldsymbol{J}(\boldsymbol{q})_x \\ \boldsymbol{J}(\boldsymbol{q})_\theta \end{bmatrix}. \tag{8}$$

Here, $\boldsymbol{J}(\boldsymbol{q})_x \in \mathbb{R}^{3\times n}$ maps the joint velocities $\dot{\boldsymbol{q}} \in \mathbb{R}^n$ to translational end-effector velocities and $\boldsymbol{J}(\boldsymbol{q})_\theta \in \mathbb{R}^{3\times n}$ maps $\dot{\boldsymbol{q}}$ to rotational end-effector velocities. In order to define the controller, three reference frames were defined: a fixed base frame denoted $\Sigma_b$ (this is displayed in Fig. 1 as $x$, $y$, and $z$), a moving frame fixed to the center of the U-joint (which was taken to be the robot's end-effector), denoted $\Sigma_e$, and a frame moving with the LBR robot's zero-force trajectory, denoted $\Sigma_0$. Both, $\boldsymbol{J}(\boldsymbol{q})_x$ and $\boldsymbol{J}(q)_\theta$ were expressed with respect to the end-effector frame $\Sigma_e$. For the end-effector translational impedance controller, the desired control torque $\boldsymbol{\tau}_x \in \mathbb{R}^n$ was computed by

$$\boldsymbol{\tau}_x = \boldsymbol{J}(\boldsymbol{q})_x^T \left(\boldsymbol{K}_x(\boldsymbol{x}_0 - \boldsymbol{x}) - \boldsymbol{B}_x\dot{\boldsymbol{x}}\right). \tag{9}$$

$\boldsymbol{\tau}_x \in \mathbb{R}^n$ described a translational spring-damper system with linear stiffness $\boldsymbol{K}_x \in \mathbb{R}^{3\times 3}$ and linear damping $\boldsymbol{B}_x \in \mathbb{R}^{3\times 3}$.

Authorized licensed use limited to: MIT Libraries. Downloaded on February 09,2022 at 17:31:09 UTC from IEEE Xplore. Restrictions apply.

Both $\boldsymbol{K}_x$ and $\boldsymbol{B}_x$ were chosen to be diagonal matrices. The virtual spring was attached between $\Sigma_e$ and $\Sigma_0$ frame. The position of the end-effector $\boldsymbol{x} \in \mathbb{R}^3$ and the zero-force position $\boldsymbol{x}_0 \in \mathbb{R}^3$ were represented in the base frame coordinates $\Sigma_b$. The zero force trajectory $\boldsymbol{x}_0$ moved with constant speed around a circular path with a radius of 0.1 m. For the end-effector rotational impedance controller, the desired control torque $\boldsymbol{\tau}_\theta \in \mathbb{R}^n$ was computed with

$$\boldsymbol{\tau}_\theta = \boldsymbol{J}(\boldsymbol{q})_\theta^T \left( \boldsymbol{K}_\theta \hat{\boldsymbol{u}}_0 \theta_0 - \boldsymbol{B}_\theta \dot{\theta} \right). \tag{10}$$

The rotational torque $\boldsymbol{\tau}_\theta$ aligned the axes of frame $\Sigma_e$ and moving frame $\Sigma_0$. The rotation between $\Sigma_e$ and $\Sigma_0$ was expressed by the rotation matrix ${}^0\boldsymbol{R}_e \in SO(3)$. To calculate the rotational torque $\boldsymbol{\tau}_\theta \in \mathbb{R}^n$, ${}^0\boldsymbol{R}_e$ was converted to axis-angle representation, with unit axis $\hat{\boldsymbol{u}}_0 \in \mathbb{R}^3$ and angle $\theta_0 \in \mathbb{R}$ [61], [62]. Thus, a virtual rotational spring with rotational stiffness $\boldsymbol{K}_\theta \in \mathbb{R}^{3\times3}$ was attached around $\hat{\boldsymbol{u}}_0$ to rotate about $\theta_0$. The rotational velocity $\dot{\boldsymbol{\theta}} \in \mathbb{R}^3$ was damped with dissipating element $\boldsymbol{B}_\theta \in \mathbb{R}^{3\times3}$. Note that all vectors and matrices of (9) and (10) were expressed in $\Sigma_b$. The stiffness in the $z$-direction was chosen to ensure the robot maintained contact with the sleeve bearing in all trials. Finally, the translational and rotational end-effector torques were combined

$$\boldsymbol{\tau}_e = \boldsymbol{\tau}_x + \boldsymbol{\tau}_\theta. \tag{11}$$

A diagonal $\boldsymbol{K}_\theta$ and $\boldsymbol{B}_\theta$ were chosen to approximate a constant damping ratio for each rotational direction in the end-effector impedance controller. The damping ratio along each of the three rotational directions was roughly approximated as

$$\zeta_i = \frac{b_i}{2m_i\sqrt{k_i/m_i}}. \tag{12}$$

Here, $b_i$ and $k_i$ represent the $i$th diagonal elements of $\boldsymbol{B}_\theta$ and $\boldsymbol{K}_\theta$, respectively, and $m_i$ is one of the corresponding three diagonal elements of the rotational end-effector mass matrix $\boldsymbol{\Lambda}_\theta \in \mathbb{R}^{3\times3}$ [63], given by

$$\boldsymbol{\Lambda}_\theta = \left( \boldsymbol{J}_\theta(\boldsymbol{q})(\boldsymbol{M}(\boldsymbol{q}))^{-1}\boldsymbol{J}_\theta(\boldsymbol{q})^T \right)^{-1} \tag{13}$$

where $\boldsymbol{M}(\boldsymbol{q}) \in \mathbb{R}^{n\times n}$ is the manipulator mass matrix. Given our choice for the values of $k_i$, the values of $b_i$ were chosen to yield $\zeta_i \approx 0.4$. This was a reasonable balance between an undamped ($\zeta = 0$) and critically damped ($\zeta = 1$) behavior.

For the joint-space impedance controller, the commanded torque $\boldsymbol{\tau}_q \in \mathbb{R}^n$ was expressed by

$$\boldsymbol{\tau}_q = \boldsymbol{K}_q(\boldsymbol{q}_0 - \boldsymbol{q}) - \boldsymbol{B}_q\dot{\boldsymbol{q}} \tag{14}$$

with joint-space stiffness $\boldsymbol{K}_q \in \mathbb{R}^{n\times n}$ and joint-space damping $\boldsymbol{B}_q \in \mathbb{R}^{n\times n}$. The nominal joint position $\boldsymbol{q}_0 \in \mathbb{R}^n$ was constant throughout the trial and corresponded to a robot end-effector position at the origin of $\Sigma_b$ with a $15^\circ$ rotation about both the $x$ and $y$ axes. This configuration was chosen so that the joint-space impedance controller always conflicted with the end-effector impedance controller. The nominal joint-space pose was $\boldsymbol{q}_0 = [-56.16, -47.4, 87.7, 83.2, -42.1, -71.9, 28.8]^T$ (degrees) and is shown in Fig. 2. $\boldsymbol{B}_q$ was chosen as a function of $\boldsymbol{K}_q$ to yield an approximate damping ratio of 0.32 to 0.42 along each joint. This was done in a manner similar to (12), but with $k_i$, $b_i$, and $m_i$ being each of the seven diagonal entries of $\boldsymbol{K}_q$, $\boldsymbol{B}_q$, and $\boldsymbol{M}(\boldsymbol{q})$, respectively.

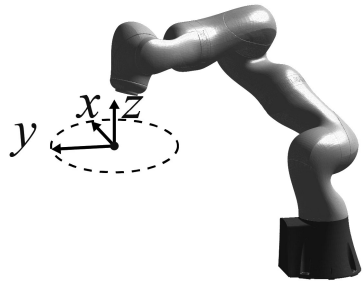


Fig. 2. Nominal joint-space position ($\boldsymbol{q}_0$) used in the experiments.

Finally, to vary the nullspace dimension, we composed the subcontrollers in two ways: using the complete 6-D rotational and translational end-effector torque $\tau_e$, yielding a 1-D nullspace; or using only the 3-D translational end-effector torque $\tau_x$, yielding a 4-D nullspace. The nullspace projectors were modified as follows in the 1-D and 4-D nullspace cases

$$\boldsymbol{\tau}_{1\text{D}} = \underbrace{\boldsymbol{\tau}_e}_{\text{Task 1}} + \underbrace{\boldsymbol{N}_{1\text{D}}\boldsymbol{\tau}_q}_{\text{Task 2}} \tag{15a}$$

and

$$\boldsymbol{\tau}_{4\text{D}} = \underbrace{\boldsymbol{\tau}_x}_{\text{Task 1}} + \underbrace{\boldsymbol{N}_{4\text{D}}\boldsymbol{\tau}_q}_{\text{Task 2}}. \tag{15b}$$

Here, the nullspace projector $\boldsymbol{N}_{1\text{D}} \in \mathbb{R}^{n\times n}$ is defined using the complete Jacobian matrix by

$$\boldsymbol{N}_{1\text{D}} = \boldsymbol{I} - \boldsymbol{J}(q)^T(\boldsymbol{J}(q)^\#)^T \tag{16a}$$

to project the torques of the joint-space impedance controller (Task 2) into the nullspace of the 6-D end-effector impedance controller (Task 1). The nullspace projector $\boldsymbol{N}_{4\text{D}} \in \mathbb{R}^{n\times n}$ is defined using only the translational component of the Jacobian matrix by

$$\boldsymbol{N}_{4\text{D}} = \boldsymbol{I} - \boldsymbol{J}(q)_x^T(\boldsymbol{J}(q)_x^\#)^T. \tag{16b}$$

Likewise, it projects the torques of the joint-space impedance controller (Task 2) into the nullspace of the 3-D end-effector impedance controller (Task 1).

### C. Test Conditions

The performance of impedance superposition ($\boldsymbol{W}^{-1} = \boldsymbol{0}$) and a conventional choice of nullspace projector ($\boldsymbol{W} = \boldsymbol{I}$) was evaluated under several test conditions. First, each condition was tested when the circular constraint was OFF and when it was ON, denoted "unconstrained" and "constrained," respectively. Second, in each case the nullspace dimension was either one or four. Third, the influence of the LBR controller parameters was investigated. Fourth, to compare nullspace projection methods, the effect of weighting matrix was evaluated. Each of these conditions is described in detail in this section; a summary is presented in Table II.

Authorized licensed use limited to: MIT Libraries. Downloaded on February 09,2022 at 17:31:09 UTC from IEEE Xplore. Restrictions apply.

TABLE II
TEST CONDITIONS AND NOTATIONS IN THIS ARTICLE

| Condition | Parameter | Notation |
|---|---|---|
| | LBR | |
| Weighting Matrix $\boldsymbol{W}$ | See methods | $\mathbf{0}$, $\boldsymbol{I}$, $\boldsymbol{M}(\boldsymbol{q})$, $\boldsymbol{B}_q$, $\boldsymbol{K}_q$ |
| Nullspace Dimension | $n-m=1$ | 1D |
| | $n-m=4$ | 4D |
| Controller | $\boldsymbol{K}_q$, 13 $s/rev$ | Standard |
| | $\boldsymbol{K}_q$, 4 $s/rev$ | Fast Speed |
| | $\boldsymbol{K}_{q,low}$, 13 $s/rev$ | Low Stiffness |
| | InMotion | |
| Circular constraint | – | Unconstrained |
| | radius 0.08 $m$ | Constrained |

TABLE III
CONTROLLER PARAMETERS

| Variable | Values | Units |
|---|---|---|
| $\boldsymbol{K}_x$ | diag([1800, 1800, 2000]) | N/m |
| $\boldsymbol{B}_x$ | diag([43.3, 31.68, 37.19]) | N-s/m |
| $\boldsymbol{K}_\theta$ | diag([260, 260, 100]) | N/rad |
| $\boldsymbol{B}_\theta$ | diag([3.0, 3.4, 1.6]) | N-s/rad |
| $\boldsymbol{K}_q$ | diag([10, 10, 10, 10, 5, 5, 1]) | N-m/rad |
| $\boldsymbol{B}_q$ | diag([2.5, 3.6, 2.1, 2.1, 0.3, 0.2, 0.1]) | N-m-s/rad |
| $\boldsymbol{K}_{q,low,1D}$ | $0.1\boldsymbol{K}_q$ | N-m/rad |
| $\boldsymbol{B}_{q,low,1D}$ | $\sqrt{0.1}\boldsymbol{B}_q$ | N-m/rad |
| $\boldsymbol{K}_{q,low,4D}$ | $0.3\boldsymbol{K}_q$ | N-m/rad |
| $\boldsymbol{B}_{q,low,4D}$ | $\sqrt{0.3}\boldsymbol{B}_q$ | N-m/rad |

All nondiagonal stiffness and damping terms were zero.

*1) Circular Constraint:* In all conditions, the LBR was coupled to the InMotion with a U-joint and bearing system described above. In the unconstrained trials, the InMotion robot was turned OFF; it remained passive and highly back-drivable, but still coupled to the LBR. In the constrained trials, the InMotion robot enforced a circular constraint (radius = 0.08 m). This constraint was enforced by an impedance controller, with a normal stiffness of 2500 N/m, and a normal damping of 40 N · m/s. The accuracy of rendering the constraint was verified by kinematic and end-point force/torque measurements obtained from the InMotion robot. The differing radii of the LBR's zero-force position (0.1 m) and the constrained circular path enforced by the InMotion robot ensured that the observed behavior occurred under conditions of significant forceful contact. In all experiments, the InMotion encoders and force transducer were used to record the planar interaction-point positions and interaction forces presented herein.

*2) Nullspace Dimension:* For all experiments, Task 2, the nullspace-projected joint-space impedance controller, was always active. However, the number of dimensions in Task 1 was varied. In some experiments, only the end-effector translational impedance controller was applied (16b). This meant that the end-effector task was 3-D, resulting in a 4-D nullspace. For other experiments, both the translational and rotational controllers of (16a) were applied. This resulted in a 6-D end-effector task, leaving a 1-D nullspace.

*3) Weighting Matrix:* To quantify performance differences due to the choice of weighting matrix $\boldsymbol{W}$, five different weighting matrices were tested: $\mathbf{0}$, $\boldsymbol{I}$, $\boldsymbol{M}(\boldsymbol{q})$, $\boldsymbol{B_q}$, and $\boldsymbol{K_q}$. A weighting matrix choice of $\boldsymbol{W}^{-1}=\mathbf{0}$ results in $\boldsymbol{N}=\boldsymbol{I}$; this is the case of simple superimposition of the end-effector and joint-space tasks, without a nullspace projector. We initially compared that case to a representative weighting matrix $\boldsymbol{W}=\boldsymbol{I}$, which corresponds to the well-known Moore–Penrose pseudoinverse [53]. Subsequently, performance with the other weighting matrices was quantified.

*4) Controller:* To understand the influence of robot inertial dynamics and the joint-space impedance controller used to manage redundancy, three conditions were examined: moderate joint-space stiffness and slow speed (13 s/rev), which is hereafter referred to as a "standard" condition; moderate joint-space stiffness and fast speed (4 s/rev); and low joint-space stiffness and slow speed. A period of 13 s/rev was extremely slow; at this speed, all dynamic effects were negligible, the motion was quasi-static, and behavior was dominated by the controller stiffness. If joint-space stiffness is sufficiently large relative to task-space stiffness, managing redundancy using joint-space impedance will substantially interfere with the end-effector task. In this work, the "moderate" joint-space stiffness was chosen to be large enough to cause substantial deviation from the desired end-effector task (more than 10 cm when unconstrained and more than 10 N when constrained) when the impedances were superimposed (i.e., the $\mathbf{0}$ projector case). The fast speed, a period of 4 s/rev, was chosen to elicit significant dynamic effects due to the robot's inertial dynamics. Quantitative analysis of the quasi-static versus dynamic speeds is presented in Appendix A.

To test whether a nullspace projection is even required in the first place, a low joint-space stiffness condition was included, executed at the slow speed (13 s/rev). This stiffness was chosen to be the smallest value that would "manage the redundancy" of the robot within a single cycle. If a large joint-space position disturbance was applied to the LBR arm, it would return to a set of joint angles near the nominal joint configuration within one crank-turning cycle. This low joint-space stiffness and damping differed when the nullspace dimension varied; the exact values used are reported in Table III.

### D. Data Analysis

In each trial, the LBR completed two separate motions of three revolutions each. The abrupt engagement of the robot controller

Authorized licensed use limited to: MIT Libraries. Downloaded on February 09,2022 at 17:31:09 UTC from IEEE Xplore. Restrictions apply.

at the start of each motion induced transient behavior in the robot end-effector motion as task 1 was not critically damped. To eliminate possible transients from the data analysis, the first revolution in each of these trials was discarded.

In the standard condition, since the robot moved quasi-statically, dominated by stiffness, the robot was expected to closely follow the target position of the end-effector impedance controller when a nullspace projector was used. To quantify errors in position, the displacement normal to the closest point on the circle was computed

$$\Delta x = 0.1 - r_n \tag{17}$$

where 0.1 m was the desired distance from the origin and $r_n = \sqrt{x^2 + y^2}$ was distance from the origin to the actual robot position. This was the dependent measure for the unconstrained case.

In the constrained condition, the radius of the zero-force LBR path was $x_0 = 0.1$ m, while the radius of the InMotion's virtual constraint was 0.08 m. Thus, the LBR robot was expected to move in a perfect circle at a radius determined by equilibrium between the stiffnesses of the LBR and InMotion robots. This required a constant normal force of 20.93 N to be exerted on the InMotion handle. Positive normal force denoted an outward-directed force exerted on the InMotion handle, away from the circular constraint center; conversely, negative normal force was directed inward, toward the constraint center. Thus, the dependent measure in the constrained condition was the deviation of the measured normal force from the expected normal force

$$\Delta f = 20.93 - f_n. \tag{18}$$

For each of the dependent measures, the root-mean-squared-error (RMSE) was computed for four crank cycles. While this metric was expected to approach zero only in the quasi-static case, it was also applied to the fast trials, even though the dynamic effects were expected to be significant and result in a nonzero mean force error, e.g., due to the centrifugal acceleration. Nevertheless, it remained a suitable metric with which to compare the behaviors of different projector choices and nullspace dimensions.

### *E. Statistical Analysis*

The difference of RMSE between the superposition of mechanical impedance ($\boldsymbol{W}^{-1} = \boldsymbol{0}$) and a standard nullspace projector ($\boldsymbol{W} = \boldsymbol{I}$) was computed. This difference was denoted RMSE $\boldsymbol{0} - \boldsymbol{I}$. When unconstrained, the RMSE difference was computed in terms of position; when constrained, the RMSE difference was computed in terms of normal force. For both the unconstrained and constrained conditions, a two-way analysis of variance (ANOVA) was performed. The ANOVA assessed the effect of nullspace dimension (1-D or 4-D) and controller condition (moderate stiffness, slow; moderate stiffness, fast; or low stiffness, slow) on the RMSE difference. For both the unconstrained and constrained results, three post-hoc two-sample *t*-tests were performed to determine if a significant difference existed between the 1-D and 4-D conditions. Two post-hoc one-sample *t*-tests were performed to determine if impedance superposition was significantly different from nullspace projection in the constrained 4-D nullspace standard and fast conditions.

In this work, statistical analysis aimed to assess differences between multiple conditions, each of which possessed more than one level. To avoid Type I errors (false positive) associated with performing multiple *t*-tests, ANOVA was first employed to determine if statistically significant differences between the means existed. The test statistic used by ANOVA is described by the F-distribution. The results present the F-statistic, its associated degrees of freedom, and the probability of a nonsignificant effect. The analysis used in this work is described in several standard texts, e.g., [64].

The differences of RMSE between the identity weighting matrix ($\boldsymbol{W} = \boldsymbol{I}$) and all other weighting matrices ($\boldsymbol{M}(\boldsymbol{q})$, $\boldsymbol{B}$, and $\boldsymbol{K}$) were computed. These differences were denoted RMSE $\boldsymbol{I} - \boldsymbol{W}$. For each nullspace dimension and constraint condition, a two-way ANOVA was performed to assess the effect of nullspace weighting matrix ($\boldsymbol{M}(\boldsymbol{q})$, $\boldsymbol{B}$, or $\boldsymbol{K}$) and controller condition (moderate stiffness, slow; moderate stiffness, fast; or low stiffness, slow). Post-hoc one-sample *t*-tests were run to identify significant differences between in RMSE $\boldsymbol{I} - \boldsymbol{W}$.

## III. RESULTS

In this section, the unconstrained results in the standard condition (slow, moderate stiffness) are presented first. Next, constrained results in the standard condition are shown. Third, the results of fast, moderate stiffness trials are reported. Fourth, results with low joint-space stiffness and slow speed are presented. Finally, a comparison of different nullspace weighting matrices is reported.

### *A. Standard Condition, Unconstrained*

In the unconstrained condition, the InMotion robot did not enforce a circular constraint. However, the InMotion robot remained passively coupled to the LBR with the U-joint and bearing system. With no constraint, we hypothesized that when the robot was operating with a nonzero nullspace projection weighting matrix, there would be no disruption of Task 1 from Task 2, regardless of whether the nullspace had one dimension or four. The trajectory was expected to be close to or even overlay the circular robot path $\boldsymbol{x}_0$ (bold dashed line in Fig. 3) and with $\boldsymbol{W} = \boldsymbol{I}$, this was indeed observed.

In the $\boldsymbol{W}^{-1} = \boldsymbol{0}$ case, superimposing impedances was expected to result in conflict between Tasks 1 and 2, leading to significant tracking errors in Task 1. This was observed in the 1-D nullspace condition (see Fig. 3 top left). The $\boldsymbol{W}^{-1} = \boldsymbol{0}$ case (blue line) substantially deviated from the circular trajectory of the LBR end-effector task, as indicated by the bold dashed line.

While it was expected that Task 2 would visibly conflict with Task 1 in the absence of a valid nullspace projector, one unexpected result was that when the dimension of the nullspace was increased from one to four (by removing the rotational impedance controller from Task 1), the task conflict was substantially reduced. This can be seen in Fig. 3 (top middle).

Authorized licensed use limited to: MIT Libraries. Downloaded on February 09,2022 at 17:31:09 UTC from IEEE Xplore. Restrictions apply.

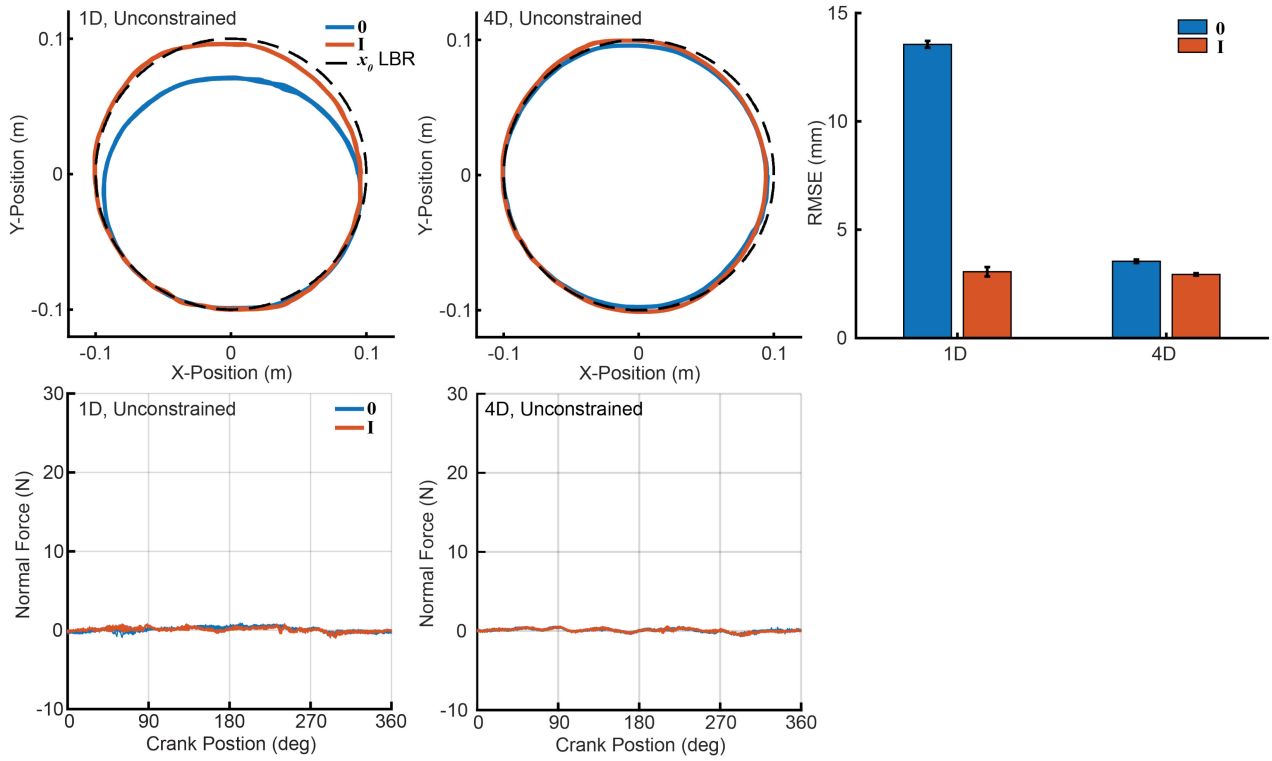


Fig. 3. *Standard condition, unconstrained*: 1-D nullspace (left column) and 4-D nullspace (middle column). Trajectory plots (top left and top middle) and the zero-force path of the LBR (bold dashed line). Normal force plots (bottom left and bottom middle). Position RMSE (top right). The superposition of mechanical impedance is denoted by $\boldsymbol{W}^{-1} = \mathbf{0}$ (blue) and the Moore–Penrose inverse denoted $\boldsymbol{W} = \boldsymbol{I}$ (red). The superposition of mechanical impedances was substantially less disruptive with a 4-D nullspace.

To assess quantitative differences in the unconstrained trials, the RMSE of the robot position was computed. This provided a measure of the deviation from expected behavior as seen in Fig. 3 (top right) and quantified the qualitative observations. Remarkably, for both the 1-D and 4-D nullspace conditions, there appeared to be no appreciable difference between the various nonzero projectors. In the 1-D nullspace case, the zero projector (impedance superposition) introduced substantial task conflict, while in the 4-D nullspace case, the RMSE it evoked was not appreciably higher than any of the other projectors. These differences are compared statistically in Section III-E.

### B. Standard Condition, Constrained

In the constrained condition, both force and motion must be considered. In this experiment, the virtual constraint radius enforced by the InMotion was 0.08 m and the diameter of the zero-force robot path was 0.1 m. Thus, the LBR was expected to move along a constant radius circle between the InMotion (dotted) and LBR (dashed) lines in Fig. 4 (top). In the standard trials, the motion was quasi-static, well within the stiffness-dominated regime, meaning that all dynamic effects were negligible (Appendix A). The displacement of the handle from its zero-force path was determined by the relative stiffness of the two robots and a constant normal force should have been exerted.

As expected, with a 1-D nullspace the superposition of joint-space stiffness substantially disrupted the LBR task-space position and normal force (the solid blue line in the top two panels of Fig. 4). The disruption of the task was sufficient for the robot occasionally to exert inward normal forces on the virtual constraint. Inward (compressive) normal forces exerted on a constraint surface are inherently destabilizing [65]. This demonstrates that superposition of joint-space and task-space mechanical impedance may, in some cases, lead to static instability and potential safety concerns.

As with the unconstrained case, the superposition of mechanical impedance ($\boldsymbol{W}^{-1} = \mathbf{0}$) performed substantially better with a 4-D nullspace as seen in Fig. 4. These differences are compared statistically in Section III-E.

### C. Fast Motion

Fast motions were tested to elicit behavior in which inertial dynamics were substantial. With a 1-D nullspace, both impedance superposition $\boldsymbol{W}^{-1} = \mathbf{0}$ and nullspace projection $\boldsymbol{W} = \boldsymbol{I}$ showed visible deviations from nominal motion when unconstrained (see Fig. 5, top left) and from nominal force when constrained (see Fig. 5, bottom left). With a 4-D nullspace, these deviations were substantially reduced, both motions when unconstrained (Fig. 5, top middle) and forces when constrained (Fig. 5, bottom middle). A comparison of RMSE for position is shown in Fig. 5, top right and force in Fig. 5, bottom right. While impedance superposition was clearly inferior with a 1-D nullspace, that disadvantage was nearly eliminated by the

Authorized licensed use limited to: MIT Libraries. Downloaded on February 09,2022 at 17:31:09 UTC from IEEE Xplore. Restrictions apply.

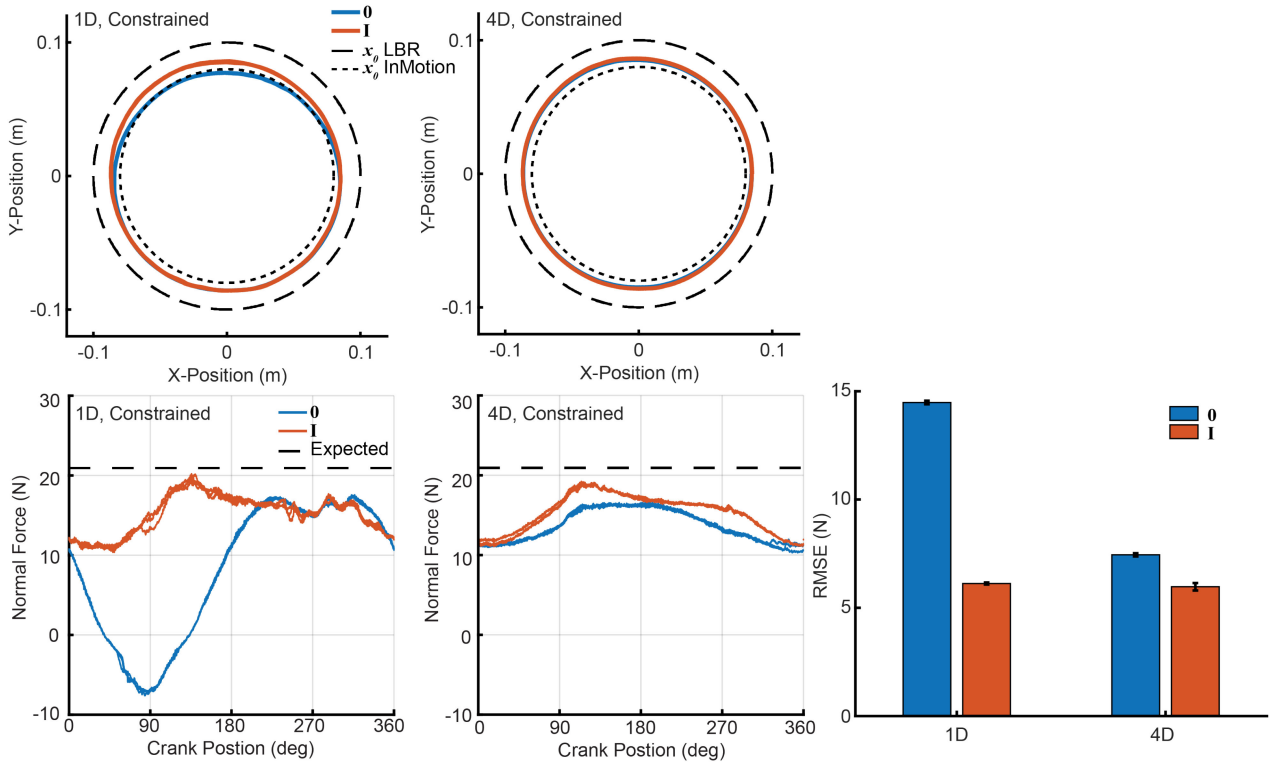


Fig. 4. *Standard condition, constrained*: 1-D nullspace (left column) and 4-D nullspace (middle column). Trajectory plots (top left and top middle), the zero-force path of the LBR (bold dashed line), and the zero-force path of the InMotion (dotted line). Normal force plots (bottom left and bottom middle) and the expected normal force (bold dashed line). Normal force RMSE (bottom right). The superposition of mechanical impedance is denoted by $\boldsymbol{W}^{-1} = \mathbf{0}$ (blue) and the Moore–Penrose inverse denoted $\boldsymbol{W} = \boldsymbol{I}$ (red). With a 4-D nullspace, the superposition of mechanical impedances was substantially less disruptive.

4-D nullspace. These differences are compared statistically in Section III-E.

### *D. Low Joint-Space Stiffness*

For a redundant robot, one way of achieving a predictable motion is to assign joint-space impedances that affect the nullspace motion of the robot in a repeatable manner. As can be seen in Sections III-A and III-B, these impedances may cause a conflict between Task 1 and Task 2. Of course, the smaller the joint-space impedance, the smaller the task conflict. However, as the joint-space stiffness is reduced, external perturbations or small errors in friction compensation may cause the redundant degrees of freedom to deviate from the nominal configuration. This may lead to unpredictable or undesirable behavior; for example, joint-space drift may cause the robot to reach joint limits. In this experiment, we aimed to determine if an acceptable compromise between these two competing factors could be achieved. We tested whether joint-space stiffness could be made small enough to reduce task-space disruption to acceptable levels, yet large enough to ensure desirable behavior. In this experiment, the joint-space stiffness of Task 2 was reduced to the point where it was still sufficient to restore the nominal joint-space configuration within one cycle of motion. The exact parameters used are presented in Table III.

The results of using this lower joint-space stiffness can be seen in Fig. 6. In the unconstrained case with a 1-D nullspace, impedance superposition still resulted in greater RMSE position errors than nullspace projection, though, as expected, to a much lesser degree. With a 4-D nullspace, any difference became negligible. These differences are compared statistically in Section III-E.

### *E. Statistical Comparisons*

The RMSE $\mathbf{0} - \boldsymbol{I}$ for the position in the unconstrained case showed a significant main effect of nullspace dimension ($F_{1,18} = 8148.94$, $P \ll 0.001$), a main effect of controller ($F_{2,18} = 2494.55$, $P \ll 0.001$), and a significant interaction between nullspace dimension and controller ($F_{2,18} = 1886.36$, $P \ll 0.001$). Posthoc two-sample *t*-tests identified significant differences between 1-D and 4-D nullspace dimension at the standard, fast, and low-stiffness levels of the controller conditions. Fig. 7 (left) shows that the interaction was clearly due to a greater sensitivity to controller with a 1-D nullspace. Thus, the effect of increasing nullspace dimension was significant and substantial.

The RMSE $\mathbf{0} - \boldsymbol{I}$ for normal force in the constrained case showed a significant main effect of nullspace dimension ($F_{1,18} = 9960.34$, $P \ll 0.001$), a main effect of controller ($F_{2,18} = 3672.30$, $P \ll 0.001$), and an interaction between nullspace dimension and controller ($F_{2,18} = 2078.45$, $P \ll 0.001$). Post-hoc two-sample *t*-tests identified significant differences between 1-D and 4-D nullspace dimensions at the standard

Authorized licensed use limited to: MIT Libraries. Downloaded on February 09,2022 at 17:31:09 UTC from IEEE Xplore. Restrictions apply.

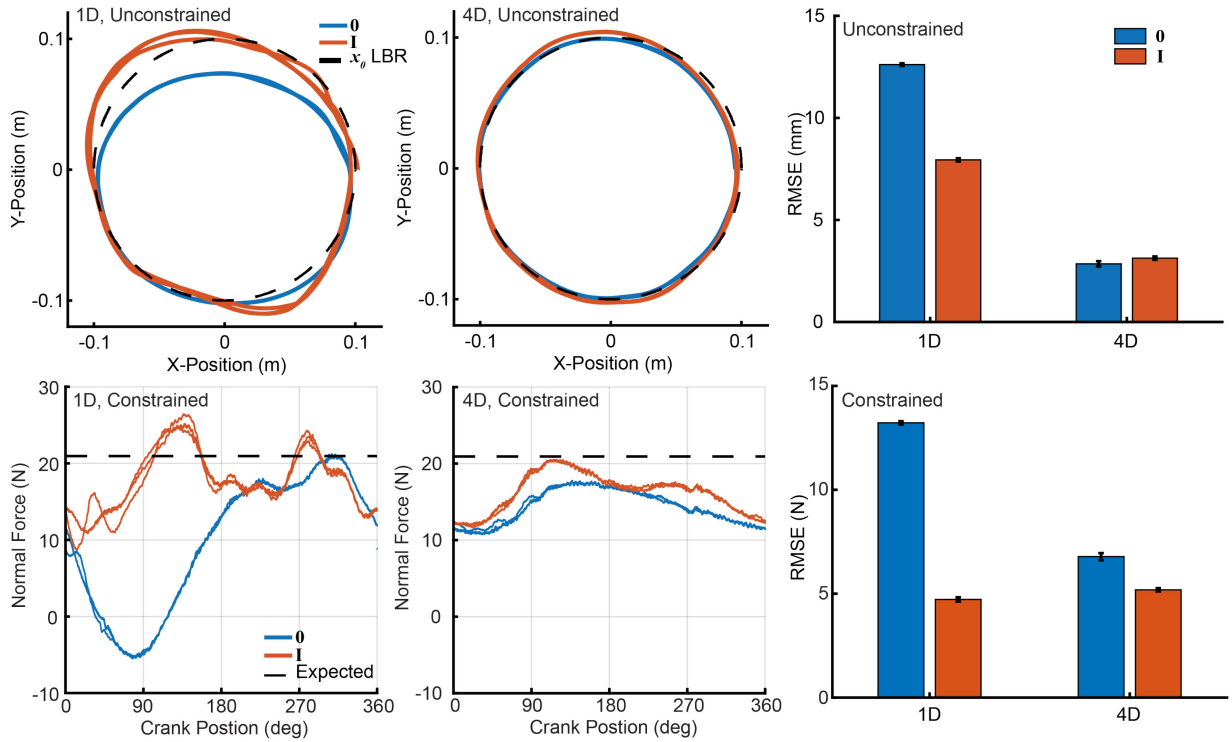


Fig. 5. *Fast motion*: Comparison of unconstrained (top row) and constrained (bottom row) trials with impedance superposition ($\boldsymbol{W}^{-1} = \boldsymbol{0}$) and nullspace projection $\boldsymbol{W} = \boldsymbol{I}$. Trajectories are presented for the unconstrained trials and normal forces for the constrained trials. Performance with a 1-D nullspace is shown in the left column and with a 4-D nullspace in the middle column. The right column compares the RMSE of position (unconstrained) and normal force (constrained). With a 4-D nullspace, comparable position errors and force errors were achieved with impedance composition.

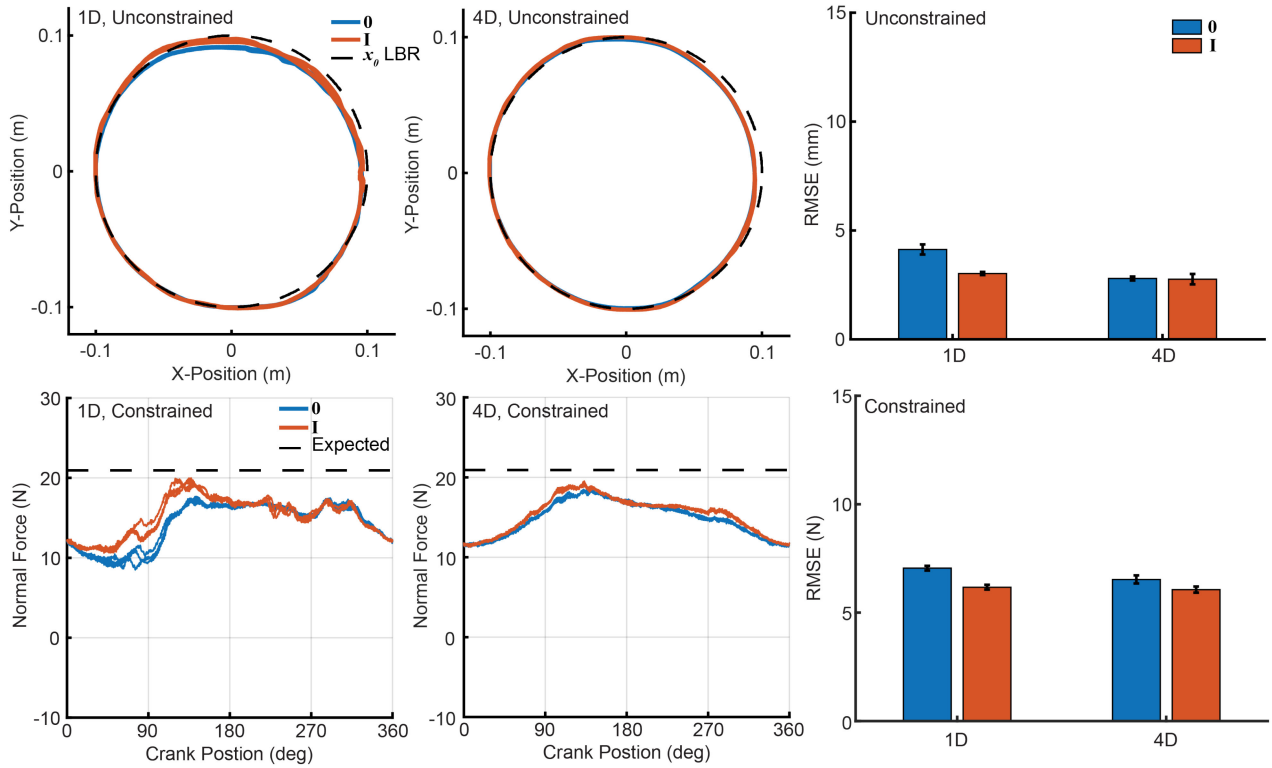


Fig. 6. *Low stiffness condition*: Performance with low stiffness at slow speed, with a 1-D nullspace (left column) and a 4-D nullspace (middle column). Trajectories are presented in the unconstrained case (top left and top middle) and normal force in the constrained case (bottom left and bottom middle). The right column compares RMSE for position when unconstrained (top row) and force when constrained (bottom row).

Authorized licensed use limited to: MIT Libraries. Downloaded on February 09,2022 at 17:31:09 UTC from IEEE Xplore. Restrictions apply.

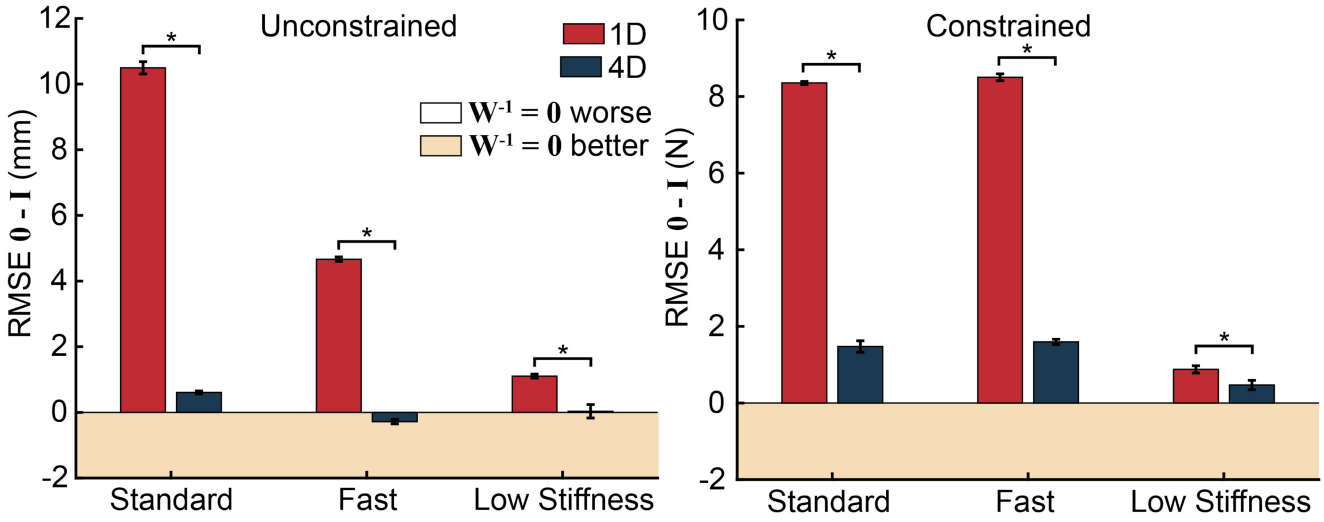


Fig. 7. Difference in root-mean-squared errors between impedance superposition and nullspace projection for different controller parameters and nullspace dimensions. * denotes statistical significance with $P < 0.05$. Left panel: RMSE $\mathbf{0} - \boldsymbol{I}$ of position for unconstrained motions; Right panel: RMSE $\mathbf{0} - \boldsymbol{I}$ of normal force for constrained conditions. With a 4-D nullspace, both position and force errors were reduced and occasionally impedance superposition was superior to nullspace projection.

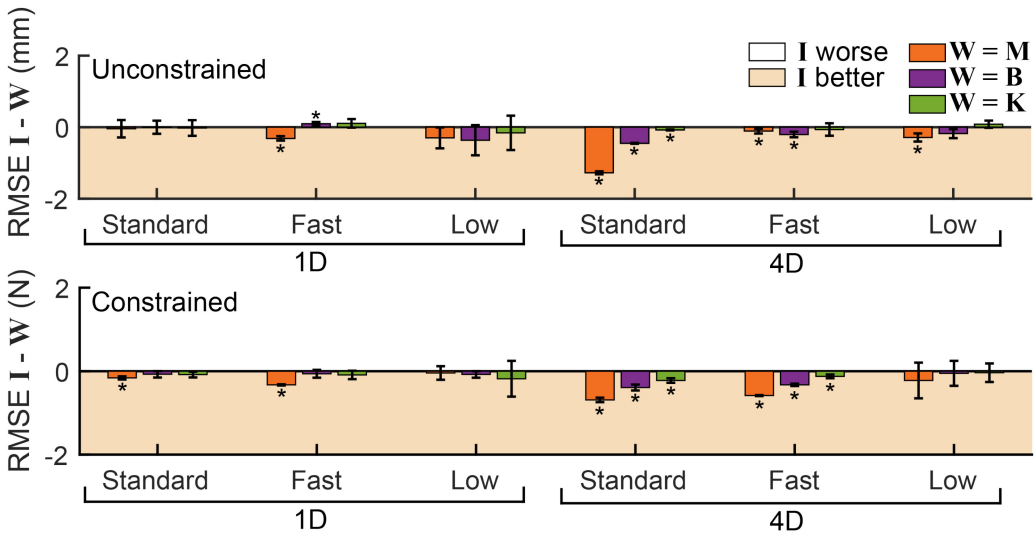


Fig. 8. RMSE $\boldsymbol{I} - \boldsymbol{W}$ of position for the unconstrained (top) and RMSE $\boldsymbol{I} - \boldsymbol{W}$ of normal force for the constrained conditions (bottom). Note that the identity weighting matrix was comparable to if not better than the other weighting matrix choices in nearly every condition.

and fast levels of controller. Clearly, the negligible difference at the low-stiffness level of the controller was the cause of the interaction as seen in Fig. 7 (right). Thus, the effect of increasing nullspace dimension on the RMSE $\mathbf{0} - \boldsymbol{I}$ normal force was significant and substantial when the joint-space stiffness was not negligible.

*1) Different Weighting Matrices:* We found no evident differences between the various nonzero null-space weighting matrices. The trajectories corresponding to the different nullspace projections all very nearly lay on top of one another. With a 4-D nullspace, there appeared to be small, systematic differences in the normal forces but they were minimal.

This was somewhat surprising. Theoretically, using $\boldsymbol{M}(\boldsymbol{q})$ weighting matrix yields a dynamically consistent nullspace projector and should therefore show superior behavior for fast robot motions [22], [55]. However, without an accurate inertial model of the robot, other projector choices may lead to superior performance in practice [18], [21], [22], [56]. In the experiments reported here, a negligible difference between projection methods was observed (see Fig. 8). Of these small differences one notable observation was that using the mass matrix, $\boldsymbol{W} = \boldsymbol{M}(\boldsymbol{q})$, was not superior—even in the fast case. Indeed, in many cases performance using the mass matrix was slightly worse than with the other choices.

Four ANOVAs were performed to assess the influence of weighting matrix and controller. With a 1-D nullspace, the RMSE $\boldsymbol{I} - \boldsymbol{W}$ for position in the unconstrained case showed no significant effects; however the main effect of controller was nearly significant ($F_{2,27} = 3.31$, $P = 0.0519$). For constrained motion, the RMSE $\boldsymbol{I} - \boldsymbol{W}$ for normal force with a 1-D nullspace showed no significant effect of weighting matrix or controller.

Authorized licensed use limited to: MIT Libraries. Downloaded on February 09,2022 at 17:31:09 UTC from IEEE Xplore. Restrictions apply.

With a 4-D nullspace, the RMSE $\boldsymbol{I} - \boldsymbol{W}$ for position in the unconstrained case showed a main effect of weighting matrix ($F_{2,27} = 95.47$, $P \ll 0.001$), a main effect of controller ($F_{2,27} = 98.45$, $P \ll 0.001$), and a significant interaction between weighting matrix and controller ($F_{4,27} = 43.77$, $P \ll 0.001$). The RMSE $\boldsymbol{I} - \boldsymbol{W}$ for the normal force showed a main effect of weighting matrix ($F_{2,27} = 11.36$, $P \ll 0.001$), and a main effect of controller ($F_{2,27} = 9.40$, $P = 0.001$). Post-hoc $t$-tests revealed that only the unconstrained fast speed $\boldsymbol{B}$ matrix condition was significantly better than the $\boldsymbol{I}$ weighing matrix. To our knowledge, this was the first time a damping matrix was used as a weighting matrix; it shows promising results.

Despite the statistical significance of some of these comparisons, the magnitude of the differences between projection methods was small (RMSE less than 1.5 mm and less than 1 N, respectively, in all cases). These values are close to the resolution of the measurement system. Furthermore, the robot variability across trials was extremely low, which increased the sensitivity of the statistical methods. Thus, while significant effects of nullspace weighting matrix were detected, these significant effects were insubstantial and mainly reflect the repeatability of the robot.

## IV. Discussion

The literature on redundancy management, particularly in the areas of reaching and manipulation, predominantly considers nullspace projection methods and their application. One direction of research focused on qualitative evaluation of weighting matrix choice in either free-space or contact tasks [9], [13], [18], [22], [27], [33], [34], [48]. Another direction of research explored large task hierarchies in which a full-rank joint-space redundancy-managing impedance plays an insignificant role at the bottom of the hierarchy [8]–[11], [22]. In most of the literature, the case of simple impedance superposition is not considered. This is presumably because, in theory, impedance superposition may cause task conflict, while the use of nullspace projectors will not. In practice, however, this may not be the case.

The goal of the present work was to investigate real kinematically redundant robots with all of their nonideal behavior, including friction, kinematic errors, etc. These robots are increasingly used to manage complex physical interaction. We aimed to quantify the performance in practice of commonly used control methods—specifically nullspace projections—and compare them with impedance superposition. The stability concerns presented by physical interaction motivate understanding any differences between theoretical and actual performance.

The experimental paradigm investigated in this work, turning a crank, embodies a number of key challenges encountered in physical interaction tasks. The first is contact and/or coupled instability; it has been known since the 1970s that a robot capable of stable unconstrained motion may become unstable on contact with a physical constraint. A well-established solution to this problem is to ensure energetic passivity of the robot's dynamic interactive behavior [66], [67]. Generally, nullspace projection approaches are not passive, since the projector only acts on the force/torque factor of the product that determines mechanical power and is not power-continuous. For this reason, energy tank methods have been applied to ensure the passivity of nullspace projection methods [40], [41]. Even if the interactive behavior is dynamically passive (by the usual definition) static instability may be induced by the curvature of a kinematic constraint. Forces applied toward the center of curvature (compressive) are statically de-stabilizing while forces applied away from the center of curvature (tensile) are statically stabilizing [65], [68]. This is an important distinction as the usual definition of passivity and its relevance to coupled stability does not encompass the static (in-)stability that may be induced by exerting forces [69]. Managing both of these challenges is a minimum requirement for safe and successful physical interaction [70], [71].

This work quantified the performance of existing controllers in practice on real hardware. We report three major findings:

1) Using different nullspace weighting matrices made no substantial difference;
2) In practice, task conflicts were still present even with nullspace projections;
3) Increasing the nullspace dimension dramatically decreased task conflicts resulting from impedance superposition.

It is important to note that, in nearly every condition, the identity weighting matrix achieved comparable or better performance than the more complex weighting matrices. In practice, there may be little need for complex nullspace projections. In this experiment, the simplest approach, identity weighting, worked equally well or better than the other options investigated. Since the identity weighting matrix facilitates computation, this result might be beneficial for controlling robots with many degrees-of-freedom based on nullspace projection methods.

In the work reported here, we implemented only two multidimensional tasks, enabling us to manipulate the "wealth" of nullspace degrees of freedom left by the first task. This allowed us to examine the impact of excess degrees of freedom between the primary task and the redundancy-management task. Additionally, we went beyond qualitative comparison, and statistically examined the impact of weighting matrix choice, task speed, impedance magnitude, and degree of task error with simple superposition in both unconstrained motion and contact scenarios. A key result of this study was that increasing the effective nullspace dimension decreased the task conflict when impedance superposition was used.

*Limitations:* There are several potential sources of artifact in this work, which include errors in the robot's kinematic model, dynamic model, friction-compensation model, and the choice of task conflict metric. Using nullspace projection, the task conflict was theoretically expected to be zero. When implementing controllers on real hardware, errors may be expected due to numerical artifact and/or imperfect low-level torque control. Both of these effects should have been small; errors observed in our experiments were much larger than could be explained by imprecise torque control. Nevertheless, the torque commands may have been influenced by the highly nonlinear effects of friction. In the experiments, the LBR's friction compensation was active to ameliorate these effects but in practice this compensation was not expected to perform perfectly. However, the same

Authorized licensed use limited to: MIT Libraries. Downloaded on February 09,2022 at 17:31:09 UTC from IEEE Xplore. Restrictions apply.

imperfections were present whether impedance superposition or nullspace projection was used. They cannot account for the differences we observed.

It may seem that the choice of impedance parameters could have influenced the results. This was avoided by experimental design. This work investigated a possible conflict between two impedance controllers. The experiment was designed such that the impedance of one controller was held constant and the other was varied. In this experiment, the end-effector impedance was fixed and two levels of joint impedance were investigated. The "standard" condition used a joint stiffness, which was deliberately chosen to be large enough to cause a task conflict in the 1-D nullspace case. The second "low joint stiffness" condition was chosen by decreasing the stiffness to the lowest value that would "resolve the redundancy" (restore unperturbed motion within one cycle of motion). The main results of the paper were observed in both the standard and low joint stiffness conditions. They cannot be dismissed as due to a fortuitous selection of impedance parameters.

Another possible source of artifact might have been the choice of metric with which to quantify task conflict. For statistical analysis, we chose to use the difference in RMSE (of position and force for unconstrained and constrained tasks, respectively) between the two controllers. This avoided any concern related to the absolute magnitude of these RMSE measures.

Another potential source of error was the model assumed by the nullspace projectors. Considering that the task conflict was observed when moving quasi-statically, dynamics could not have been the cause of artifact. All nullspace projections depend on the Jacobian, which requires a model of the robot kinematics. If the kinematic model was incorrect, a difference between the actual robot nullspace and the model robot nullspace would exist. Our observations suggest that nullspace projection may be more sensitive to errors in the kinematic model than impedance superposition. This would be consistent with previous theoretical work, which has shown that the stability and passivity of an impedance controller are remarkably insensitive to errors in the kinematic model of the robot [67].

Finally, a concern might be raised that our results were peculiar to the mechanics and kinematics of the particular robot, task, and configuration that we studied. To address this concern, we performed simulations of arguably the simplest hypothetical case that could demonstrate the influence of increasing nullspace dimension (see Appendix B). A planar 3 degree-of-freedom linkage performed a 3 degree-of-freedom end-effector task (nullspace dimension 0) and a comparable 2 degree-of-freedom end-effector task (nullspace dimension 1). Fig. 9 clearly demonstrates the substantial influence of nullspace dimension, even with idealized kinematics and zero friction. Our results are unlikely to be an accident of the particular robot, task, and configuration that we studied.

### A. Analogy to Polynomial Kernel Methods?

When the nullspace dimension was increased, a substantial decrease in task space disruption was observed. One explanation of this result may be that increasing nullspace dimension with respect to a primary task increases the number of poses that the robot can take. This makes the robot more likely to reach a configuration which will result in a smaller task conflict. This approach, which casts a low-dimensional problem into a high-dimensional space, appears loosely analogous to common-practice data-driven methods for classification. It is well known that a low-dimensional problem, which is sparsely populated can be nonlinearly cast into a higher dimensional space, e.g., using the polynomial kernel method [72]. This projection increases the likelihood that a problem, which was not linearly separable in the low-dimensional space will be linearly separable in the high-dimensional space [73]. We suspect that a similar phenomenon may account for our results but testing this speculation requires further investigation beyond the scope of this report.

### B. Applications

*1) Understanding Human Motor Control:* Humans do not simply regulate kinematics. Humans also modulate the interactive dynamics of their limbs [43]–[45]. Human limb impedance varies as a function of many factors including: muscle activation [74], movement [75], activity preparation [76], force exertion level [77], task stabilization [78], and walking gait state [79], [80]. Despite about three times as many muscles as skeletal degrees of freedom, if the human limb is viewed as an actuator configured to produce an arbitrary time-varying impedance in an arbitrary configuration, it becomes clear that the human limb is profoundly *under*actuated.

However, humans modulate impedance not only with muscle activity, but also kinematics [81], [82]. In many tasks the influence of kinematics can be more than an order of magnitude greater than muscle activity or joint torque. Thus, kinematic redundancy increases the range of impedance which the human limb can produce. The kinematic nullspace is an essential aspect of human physical interaction. Even though the work reported here was performed on a robotic platform, it demonstrated one of the many benefits of the high-dimensional skeletal anatomy that humans possess.

This substantial influence of kinematics may be the reason that several example cases, which employ simple models of impedance, have been able to describe observations of human behavior [83]–[85] and achieve human-like performance [86].

*2) Applications to Robotics:* One notable result was that there may be cases in which there is no need for a nullspace projector. Instead, the simpler approach of mechanical impedance superposition may be applied. This approach may be successful when the task dimension is small relative to the number of joint-space degrees of freedom; or when only small joint-space stiffness is required; when there are computational limitations; or when dynamic interactive behavior is prioritized over exact position or force accuracy.

However, we do not conclude that impedance superposition is always superior to nullspace projection; in fact our own results showed cases in which it was not. For moderate joint-space stiffness, there was substantial disruption of Task 1 (in end-effector space) by Task 2 (in joint-space) as intended by the experimental design. That disruption was sufficient to

Authorized licensed use limited to: MIT Libraries. Downloaded on February 09,2022 at 17:31:09 UTC from IEEE Xplore. Restrictions apply.

exert compressive forces on the constraint, which is inherently destabilizing and potentially unsafe. With sufficient end-effector stiffness, instability can be avoided and passivity preserved [66], [69]. The biological solution to this problem is that muscle stiffness increases in proportion to muscle force (one of the most robust observations about mammalian muscle) [87], [88], but it is unclear whether this is a satisfactory approach for robotic applications. With a 1-D nullspace and moderate or greater joint-space stiffness, nullspace projections may be required.

### C. Future Work

There are several directions of future work, which could provide valuable insight to the observations reported here. We highlight two of them: First, in this work only two nullspace dimensions were investigated. The nullspace dimension can be modulated in two ways, by either changing the dimension of task one or by changing the dimension of task two. This simple idea motivates a systematic experimentation or simulation to investigate these factors. Second, this experiment was specifically designed to make the task conflict easy to quantify. However, if more complex tasks are to be understood, alternative metrics for quantifying task conflicts may be required [89].

## V. Conclusion

In robotics, controlling a large number of redundant degrees of freedom has commonly been viewed as a difficult challenge to overcome, especially if control is performed via optimization-based techniques. A common approach to deal with the control of kinematically redundant robots is the nullspace projection method. A simpler alternative is based on superimposing mechanical impedances, but that approach is vulnerable to task conflict, whereas nullspace projections theoretically avoid this problem. In practice, we observed that both nullspace projections and impedance superposition resulted in measurable task conflict. This surprising observation was minimally influenced by the choice of projection weighting matrix. Remarkably, when the dimension of the nullspace increased, the superposition method showed errors that were comparable to the nullspace projection methods. With no disrespect intended to Richard Bellman, high-dimensional kinematics may be a blessing rather than a curse.

## Acknowledgment

The authors would like to thank Prof. Russell Tedrake for the loan of the Kuka robot used in this article.

## Appendix A

Many of the differences between statically consistent and dynamically consistent nullspace projectors will only be elicited if the end-effector task (Task 1) involves significant accelerations with respect to the joint-space task of the robot (Task 2). To gauge the degree to which Task 1 was dynamic with respect to Task 2, the principal natural frequencies of the joint-space task of the robot were quantified.

For any given robot configuration, the local unforced mass-spring behavior of the joint-space task can be approximated as follows:

$$\boldsymbol{M}(\boldsymbol{q})\ddot{\boldsymbol{\theta}} + \boldsymbol{K_q}\boldsymbol{\theta} = 0 \tag{19}$$

where $\boldsymbol{\theta} = \boldsymbol{q} - \Delta\boldsymbol{q}$. In order to find the natural frequencies of this system, we can assume solutions of the form:

$$\boldsymbol{\theta} = \boldsymbol{a}_i \sin(\omega_i t + \phi) \tag{20}$$

where $\boldsymbol{a}_i$ represents a single mode shape and $\omega_i$ represents the corresponding natural frequency. Substituting this into (19) yields

$$(-\omega_i^2 \boldsymbol{M}(\boldsymbol{q}) + \boldsymbol{K_q})\boldsymbol{a}_i = 0. \tag{21}$$

Rearranging this yields

$$\boldsymbol{M}(\boldsymbol{q})^{-1}\boldsymbol{K_q}\boldsymbol{a}_i = -\omega_i^2 \boldsymbol{a}_i. \tag{22}$$

This has the form of a generalized eigenvalue problem, with $\boldsymbol{a}_i$ and $-\omega_i^2$ being the eigenvectors and eigenvalues of the matrix $\boldsymbol{M}(\boldsymbol{q})^{-1}\boldsymbol{K_q}$. For each experiment, the seven mode shapes and natural frequencies were computed at each time step. For all experiments, the computed natural frequencies remained approximately similar across revolutions. The computed natural frequencies were then averaged across time steps and experiments. The natural frequencies of each mode, listed in ascending order, were $\omega_n = [0.28, 0.38, 0.81, 1.09, 2.52, 3.65, 7.13]$ (Hz). The end-effector task frequencies were 0.25 Hz for the fast case, and 0.0769 Hz for the slow case, which suggests that in the fast condition, the response was dominated by the two lowest Task 2 natural frequencies. The slow condition was clearly quasi-static with respect to Task 2.

## Appendix B

In this work, the benefit of increasing nullspace dimension was clear. However, this might have been a fortuitous accident of our experiment, performed with a particular robot in a particular configuration. In order to determine if the effect of increasing nullspace dimension was generalizable, planar simulations were performed which superimposed an end-effector impedance (task 1) and joint-space impedance (task 2).

In the 0-D nullspace condition, the task space consisted of the $x$, $y$, and $\theta$ directions ($m = 3$). In the 1-D nullspace condition, the task space consisted of the $x$- and $y$-directions ($m = 2$). Both the 0-D and 1-D conditions are graphically displayed in Fig. 9 (top). In all cases the manipulator had three joints ($n = 3$). The total length of the manipulator was 1 m and the joints were divided into three equal segments. The total mass of all of the links was 1 kg. The links were assumed to be thin rods. The stiffness parameters are reported in Table IV. Here, $\boldsymbol{J}(\boldsymbol{q})_x \in \mathbb{R}^{2\times n}$ maps the joint velocities $\dot{\boldsymbol{q}} \in \mathbb{R}^n$ to translational end-effector velocities, $\dot{\boldsymbol{x}} = [\dot{x}, \dot{y}]^T$ while $\boldsymbol{J}(\boldsymbol{q})_\theta \in \mathbb{R}^{1\times n}$ maps $\dot{\boldsymbol{q}}$ to rotational end-effector velocities, $\theta$. The torque control laws for the 0-D and 1-D cases were

$$\boldsymbol{\tau}_{0D} = \underbrace{\boldsymbol{\tau}_e}_{\text{Task 1}} + \underbrace{\boldsymbol{\tau}_q}_{\text{Task 2}} \tag{23a}$$

Authorized licensed use limited to: MIT Libraries. Downloaded on February 09,2022 at 17:31:09 UTC from IEEE Xplore. Restrictions apply.

TABLE IV
CONTROLLER PARAMETERS

| Variable | Values | Units |
|---|---|---|
| $\boldsymbol{K}_x$ | diag([500,500]) | N/m |
| $\boldsymbol{B}_x$ | $0.1\boldsymbol{K}_x$ | N-s/m |
| $\boldsymbol{K}_\theta$ | 10 | N/rad |
| $\boldsymbol{B}_\theta$ | $0.1\boldsymbol{K}_\theta$ | N-s/rad |
| $\boldsymbol{K}_q$ | diag([5, 5, 5]) | N-m/rad |
| $\boldsymbol{B}_q$ | $0.1\boldsymbol{K}_q$ | N-m-s/rad |

All nondiagonal stiffness and damping terms were zero.

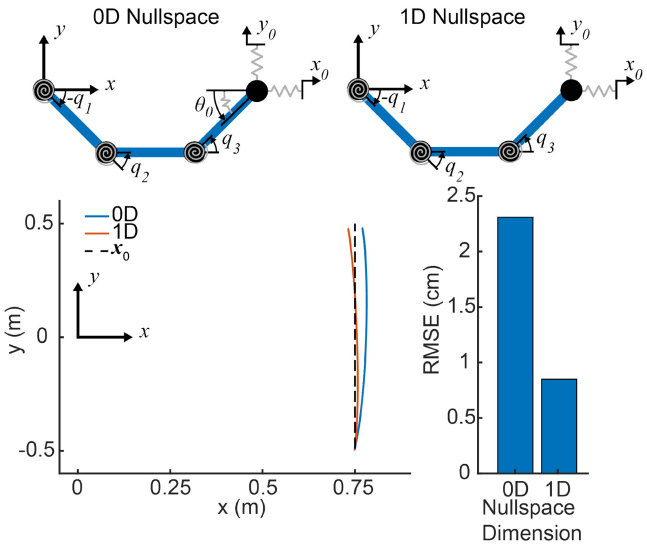


Fig. 9. Graphic depiction of a 3 degree-of-freedom manipulator with a task-space impedance controller superimposed with a joint-space impedance controller. A 3-D task space yields a 0-D nullspace (top left). A 2-D task space yields a 1-D nullspace (top right). The end-effector path when a cosine motion was tracked in the $y$-direction is shown on the bottom left. The position RMSE in the $x$-direction was much larger with a 0-D nullspace than with a 1-D nullspace (bottom right).

and

$$\boldsymbol{\tau}_{1\mathrm{D}} = \underbrace{\boldsymbol{\tau}_x}_{\text{Task 1}} + \underbrace{\boldsymbol{\tau}_q}_{\text{Task 2}}. \tag{23b}$$

The nominal joint configuration $\boldsymbol{q}_0$ was constant and is depicted in Fig. 9 (top). The task 1 horizontal position was constant ($x_0 = 0.75$ m), the task 1 orientation (only used in the 0-D nullspace condition) was constant ($\theta = 0^o$), and the task 1 vertical position was time varying ($y_0 = \frac{1}{2}\cos(2\pi t)$). The simulation was run for one cycle from $y = 0.5$ to $y = -0.5$, and back to $y = 0.5$ with a period of 35 s, which ensured the system was moving quasi-statically.

From the trajectory of the end-effector seen in Fig. 9 (bottom left), it is clear that the 1-D nullspace condition resulted in a substantial decrease of task space disruption. This is supported by the $x$-direction RMSE in Fig. 9 (bottom right).

## REFERENCES


[1] R. Bellman, "Dynamic programming," *Science*, vol. 153, no. 3731, pp. 34–37, 1966.
[2] N. Hogan, *Physical Interaction Via Dynamic Primitives*. New York, NY, USA: Springer International Publishing, 2017, pp. 269–299.
[3] N. Hogan and D. Sternad, "Dynamic primitives of motor behavior," *Biol. Cybern.*, vol. 106, no. 11-12, pp. 727–739, Dec. 2012.
[4] P. Churchland and T. Sejnowski, *The Computational Brain*, *25th Anniversary ed.*, Cambridge, MA, USA: MIT Press, 2017.
[5] G. R. Hunt, "Manufacture and use of hook-tools by new caledonian crows," *Nature*, vol. 379, no. 6562, pp. 249–251, 1996.
[6] B. Kenward, A. A. S. Weir, C. Rutz, and A. Kacelnik, "Tool manufacture by naive juvenile crows," *Nature*, vol. 433, no. 7022, pp. 121–121, 2005.
[7] E. Kandel, J. Schwartz, T. Jessell, S. Siegelbaum, and A. Hudspeth, *Principles of Neural Science*. 5th ed., *Ser. Principles of Neural Science*. New York, NY, USA: McGraw-Hill Education, 2013.
[8] G. Antonelli, F. Arrichiello, and S. Chiaverini, "Experiments of formation control with multirobot systems using the null-space-based behavioral control," *IEEE Trans. Control Syst. Technol.*, vol. 17, no. 5, pp. 1173–1182, Sep. 2009.
[9] A. Dietrich, A. Albu-Schäffer, and G. Hirzinger, "On continuous null space projections for torque-based, hierarchical, multi-objective manipulation," in *Proc. IEEE Int. Conf. Robot. Autom.*, 2012, pp. 2978–2985.
[10] A. Dietrich, C. Ott, and A. Albu-Schäffer, "Multi-objective compliance control of redundant manipulators: Hierarchy, control, and stability," in *Proc. IEEE/RSJ Int. Conf. Intell. Robots Syst.*, 2013, pp. 3043–3050.
[11] B. Siciliano and J. Slotine, "A general framework for managing multiple tasks in highly redundant robotic systems," in *Proc. 5th Int. Conf. Adv. Robot.*, vol. 2, 1991, pp. 1211–1216.
[12] L. Sentis and O. Khatib, "Synthesis of whole-body behaviors through hierarchical control of behavioral primitives," *Int. J. Humanoid Robot.*, vol. 2, no. 4, pp. 505–518, 2005.
[13] O. Khatib, "A unified approach for motion and force control of robot manipulators: The operational space formulation," *IEEE J. Robot. Autom.*, vol. 3, no. 1, pp. 43–53, Feb. 1987.
[14] A. Liegeois, "Automatic supervisory control of the configuration and behavior of multibody mechanisms," *IEEE Trans. Syst., Man, Cybern.*, vol. 7, no. 12, pp. 868–871, Dec. 1977.
[15] N. Oda, H. Ohta, T. Murakami, and K. Ohnishi, "A robust impedance control strategy for redundant manipulator," in *Proc. IECON 21st Annu. Conf. IEEE Ind. Electron.*, vol. 2, Nov. 1995, pp. 1254–1259.
[16] G. Oriolo, "Stabilization of self-motions in redundant robots," in *Proc. IEEE Int. Conf. Robot. Autom.*, May 1994, pp. 704–709, vol. 1.
[17] A. Albu-Schaffer and G. Hirzinger, "Cartesian impedance control techniques for torque controlled light-weight robots," in *Proc. IEEE Int. Conf. Robot. Autom. (Cat. No. 02CH37292).*, vol. 1, May 2002, pp. 657–663.
[18] A. Albu-Schaffer, C. Ott, U. Frese, and G. Hirzinger, "Cartesian impedance control of redundant robots: Recent results with the DLR-light-weight-arms," in *Proc. IEEE Int. Conf. Robot. Autom. (Cat. No.03CH37422)*, vol. 3, Sep. 2003, pp. 3704–3709.
[19] C. Ott, *Cartesian Impedance Control of Redundant and Flexible-Joint Robots*. Berlin, Germany: Springer, 2008.
[20] C. Ott, R. Mukherjee, and Y. Nakamura, "Unified impedance and admittance control," in *Proc. IEEE Int. Conf. Robot. Autom.*, 2010, pp. 554–561.
[21] J. Peters, M. Mistry, F. Udwadia, J. Nakanishi, and S. Schaal, "A unifying framework for robot control with redundant DOFs," *Auton. Robots*, vol. 24, no. 1, pp. 1–12, 2008.
[22] A. Dietrich, C. Ott, and A. Albu-Schäffer, "An overview of null space projections for redundant, torque-controlled robots," *Int. J. Robot. Res.*, vol. 34, no. 11, pp. 1385–1400, 2015.
[23] A. Dietrich, *Whole-Body Impedance Control of Wheeled Humanoid Robots*. Berlin, Germany: Springer, 2016.
[24] R. Platt, M. Abdallah, and C. Wampler, "Multiple-priority impedance control," in *Proc. IEEE Int. Conf. Robot. Autom.*, 2011, pp. 6033–6038.
[25] H. Sadeghian, M. Keshmiri, L. Villani, and B. Siciliano, "Null-space impedance control with disturbance observer," in *Proc. IEEE/RSJ Int. Conf. Intell. Robots Syst.*, 2012, pp. 2795–2800.
[26] H. Sadeghian, L. Villani, M. Keshmiri, and B. Siciliano, "Dynamic multi-priority control in redundant robotic systems," *Robotica*, vol. 31, no. 7, pp. 1155–1167, 2013.


Authorized licensed use limited to: MIT Libraries. Downloaded on February 09,2022 at 17:31:09 UTC from IEEE Xplore. Restrictions apply.

[27] H. Sadeghian, L. Villani, M. Keshmiri, and B. Siciliano, "Task-space control of robot manipulators with null-space compliance," *IEEE Trans. Robot.*, vol. 30, no. 2, pp. 493–506, Apr. 2014.

[28] F. Ficuciello, L. Villani, and B. Siciliano, "Variable impedance control of redundant manipulators for intuitive human-robot physical interaction," *IEEE Trans. Robot.*, vol. 31, no. 4, pp. 850–863, Aug. 2015.

[29] H. Lin, M. Howard, and S. Vijayakumar, "Learning null space projections," in *Proc. IEEE Int. Conf. Robot. Autom.*, 2015, pp. 2613–2619.

[30] J. Park and O. Khatib, "Robot multiple contact control," *Robotica*, vol. 26, no. 5, pp. 667–677, 2008.

[31] B. Henze, A. Dietrich, M. A. Roa, and C. Ott, "Multi-contact balancing of humanoid robots in confined spaces: Utilizing knee contacts," in *Proc. IEEE/RSJ Int. Conf. Intell. Robots Syst.*, 2017, pp. 697–704.

[32] C. A. Klein and C. Huang, "Review of pseudoinverse control for use with kinematically redundant manipulators," *IEEE Trans. Syst., Man, Cybern.*, vol. SMC- 13, no. 2, pp. 245–250, Mar. 1983.

[33] J. Hollerbach and K. Suh, "Redundancy resolution of manipulators through torque optimization," *IEEE J. Robot. Autom.*, vol. 3, no. 4, pp. 308–316, Aug. 1987.

[34] J. Baillieul, "Kinematic programming alternatives for redundant manipulators," in*Proc. IEEE Int. Conf. Robot. Autom.*, vol. 2, Mar. 1985, pp. 722–728.

[35] B. Hu, C. L. Teo, and H. P. Lee, "Local optimization of weighted joint torques for redundant robotic manipulators," *IEEE Trans. Robot. Autom.*, vol. 11, no. 3, pp. 422–425, Jun. 1995.

[36] G. Antonelli, F. Arrichiello, and S. Chiaverini, "The null-space-based behavioral control for mobile robots," in *Proc. Int. Symp. Comput. Intell. Robot. Autom.*, 2005, pp. 15–20.

[37] G. Antonelli, F. Arrichiello, and S. Chiaverini, "Experiments of formation control with collisions avoidance using the null-space-based behavioral control," in *Proc. 14th Mediterranean Conf. Control Autom.*, 2006, pp. 1–6.

[38] G. Antonelli, F. Arrichiello, and S. Chiaverini, "Stability analysis for the null-space-based behavioral control for multi-robot systems," in *Proc. 47th IEEE Conf. Decis. Control*, 2008, pp. 2463–2468.

[39] F. Arrichiello, S. Chiaverini, G. Indiveri, and P. Pedone, "The null-space-based behavioral control for mobile robots with velocity actuator saturations," *Int. J. Robot. Res.*, vol. 29, no. 10, pp. 1317–1337, 2010.

[40] A. Dietrich, C. Ott, and S. Stramigioli, "Passivation of projection-based null space compliance control via energy tanks," *IEEE Robot. Autom. Lett.*, vol. 1, no. 1, pp. 184–191, Jan. 2016.

[41] A. Dietrich, X. Wu, K. Bussmann, C. Ott, A. Albu-Schäffer, and S. Stramigioli, "Passive hierarchical impedance control via energy tanks," *IEEE Robot. Autom. Lett.*, vol. 2, no. 2, pp. 522–529, Apr. 2017.

[42] N. Hogan, "Impedance control: An approach to manipulation," in *Proc. Amer. Control Conf.*, 1984, pp. 304–313,.

[43] N. Hogan, "Impedance control: An approach to manipulation: Part I-theory," *J. Dyn. Syst., Meas., Control*, vol. 107, no. 1, pp. 1–7, Mar. 1985.

[44] N. Hogan, "Impedance control: An approach to manipulation: Part II-implementation," *J. Dyn. Syst., Meas., Control*, vol. 107, no. 1, pp. 8–16, Mar. 1985.

[45] N. Hogan, "Impedance control: An approach to manipulation: Part III-applications," *J. Dyn. Syst., Meas., Control*, vol. 107, no. 1, pp. 17–24, Mar. 1985.

[46] D. Verdi, "A compositional approach to robotic impedance control," Master's thesis, Massachusetts Inst. Technol., Cambridge, MA, USA, 2019.

[47] T. Yoshikawa, "Manipulability and redundancy control of robotic mechanisms," in*Proc. IEEE Int. Conf. Robot. Autom.*, vol. 2, Mar. 1985, pp. 1004–1009.

[48] D. E. Whitney, "Resolved motion rate control of manipulators and human prostheses," *IEEE Trans. Man-Mach. Syst.*, vol. 10, no. 2, pp. 47–53, Jun. 1969.

[49] F. Flacco, A. De Luca, and O. Khatib, "Motion control of redundant robots under joint constraints: Saturation in the null space," in *Proc. IEEE Int. Conf. Robot. Autom.*, 2012, pp. 285–292.

[50] F. Flacco, A. De Luca, and O. Khatib, "Control of redundant robots under hard joint constraints: Saturation in the null space," *IEEE Trans. Robot.*, vol. 31, no. 3, pp. 637–654, Jun. 2015.

[51] S. Stramigioli, *Modeling and IPC Control of Interactive Mechanical Systems—A Coordinate-Free Approach, Ser. Lecture Notes in Control and Information Sciences*. London, U.K.: Springer-Verlag London Limited, 2001.

[52] J. Lachner *et al.*, "The influence of coordinates in robotic manipulability analysis," *Mechanism Mach. Theory*, vol. 146, 2020, Art. no. 103722.

[53] R. Penrose, "A generalized inverse for matrices," *Math. Proc. Cambridge Philos. Soc.*, vol. 51, no. 3, pp. 406–413, 1955.

[54] H. Bruyninckx and O. Khatib, "Gauss' principle and the dynamics of redundant and constrained manipulators," in *Proc. IEEE Int. Conf. Robot. Autom. Symp. (Cat. No. 00CH37065)*, vol. 3, Apr. 2000, pp. 2563–2568.

[55] K.-S. Chang and O. Khatib, "Manipulator control at kinematic singularities: A dynamically consistent strategy," in *Proc. IEEE/RSJ Int. Conf. Intell. Robots Syst.. Hum. Robot Interact. Cooperative Robots*, vol. 3, Aug. 1995, pp. 84–88 vol.3.

[56] J. Nakanishi, R. Cory, M. Mistry, J. Peters, and S. Schaal, "Operational space control: A theoretical and empirical comparison," *Int. J. Robot. Res.*, vol. 27, no. 6, pp. 737–757, 2008.

[57] L. A. Hosford, "Development and testing of an impedance controller on an anthropomorphic robot for extreme environment operations," Master's thesis, Massachusetts Inst. Technol., Cambridge, MA, USA, 2016.

[58] G. Schreiber, A. Stemmer, and R. Bischoff, "The fast research interface for the KUKA lightweight robot," in *Proc. IEEE Workshop Innov. Robot Control Architectures Demanding (Res.) Appl. How Modify Enhance Commercial Controllers*, 2010, pp. 15–21.

[59] N. Hogan, H. I. Krebs, A. Sharon, and J. Charnnarong, "Interactive robotic therapist," *United States Patent US 5466213*, Nov. 1995.

[60] J. Thorup, "Inertia compensation of a planar robot for human upper limb interaction," Master's thesis, Massachusetts Inst. Technol., Cambridge, MA, USA, 2018.

[61] J. Luh, M. Walker, and R. Paul, "Resolved-acceleration control of mechanical manipulators," *IEEE Trans. Autom. Control*, vol. 25, no. 3, pp. 468–474, Jun. 1980.

[62] C. Natale, *Interaction Control of Robot Manipulators: Six Degrees-of-Freedom Tasks*. B. Siciliano, O. Khatib, and F. Groen, Eds., Berlin, Germany: Springer Science & Business Media, 2003, vol. 3.

[63] O. Khatib, "Inertial properties in robotic manipulation: An object-level framework," *Int. J. Robot. Res.*, vol. 14, no. 1, pp. 19–36, 1995.

[64] G. Keppel and T. D. Wickens, *Design and Analysis: A Researcher's Handbook*. 4thed., London, U.K.: Pearson Education, Inc., 2004.

[65] D. Rancourt and N. Hogan, "Stability in force-production tasks," *J. Motor Behav.*, vol. 33, no. 2, pp. 193–204, 2001,

[66] J. E. Colgate and N. Hogan, "Robust control of dynamically interacting systems," *Int. J. Control*, vol. 48, no. 1, pp. 65–88, 1988.

[67] N. Hogan, "On the stability of manipulators performing contact tasks," *IEEE J. Robot. Autom.*, vol. 4, no. 6, pp. 677–686, Dec. 1988.

[68] D. Rancourt and N. Hogan, "The biomechanics of force production," in *Progress in Motor Control*, Berlin, Germany: Springer, 2009, pp. 645–661.

[69] J. E. Colgate, "Strictly positive real admittances for coupled stability," *J. Franklin Inst.*, vol. 329, no. 3, pp. 429–444, 1992.

[70] J. Lachner, F. Allmendinger, E. Hobert, N. Hogan, and S. Stramigioli, "Energy budgets for coordinate invariant robot control in physical human–robot interaction," *Int. J. Robot. Res.*, 2021.

[71] S. Hjorth, J. Lachner, S. Stramigioli, O. Madsen, and D. Chrysostomou, "An energy-based approach for the integration of collaborative redundant robots in restricted work environments," in *Proc. IEEE/RSJ Int. Conf. Intell. Robots Syst.*, 2020, pp. 7152–7158.

[72] R. T. Farouki, "The Bernstein polynomial basis: A centennial retrospective," *Comput. Aided Geometric Des.*, vol. 29, no. 6, pp. 379–419, 2012.

[73] T. M. Cover, "Geometrical and statistical properties of systems of linear inequalities with applications in pattern recognition," *IEEE Trans. Electron. Comput.*, vol. EC-14, no. 3, pp. 326–334, Jun. 1965.

[74] S. C. Cannon and G. I. Zahalak, "The mechanical behavior of active human skeletal muscle in small oscillations," *J. Biomech.*, vol. 15, no. 2, pp. 111–121, 1982.

[75] D. J. Bennett, J. M. Hollerbach, Y. Xu, and I. W. Hunter, "Time-varying stiffness of human elbow joint during cyclic voluntary movement," *Exp. Brain Res.*, vol. 88, no. 2, pp. 433–442, Feb. 1992.

[76] F. Lacquaniti, M. Corrozzo, and N. A. Borghese, "Time-varying mechanical behavior of multijointed arm in man," *J. Neuriophysiol.*, vol. 69, no. 5, pp. 1443–1464, 1993.

[77] E. J. Perreault, R. F. Kirsch, and P. E. Crago, "Effects of voluntary force generation on the elastic components of endpoint stiffness," *Exp. Brain Res.*, vol. 141, no. 3, pp. 312–323, Dec. 2001.

[78] E. Burdet, R. Osu, D. W. Franklin, T. E. Milner, and M. Kawato, "The central nervous system stabilizes unstable dynamics by learning optimal impedance," *Nature*, vol. 414, pp. 446–4492001.

[79] H. Lee and N. Hogan, "Time-varying ankle mechanical impedance during human locomotion," *IEEE Trans. Neural Syst. Rehabil. Eng.*, vol. 23, no. 5, pp. 755–764, Sep. 2015.


Authorized licensed use limited to: MIT Libraries. Downloaded on February 09,2022 at 17:31:09 UTC from IEEE Xplore. Restrictions apply.

[80] H. Lee, E. J. Rouse, and H. I. Krebs, "Summary of human ankle mechanical impedance during walking," *IEEE J. Transl. Eng. Health Med.*, vol. 4, 2016, Art. no. 2100407.
[81] N. Hogan, "The mechanics of multi-joint posture and movement control," *Biol. Cybern.*, vol. 52, no. 5, pp. 315–331, 1985.
[82] R. D. Trumbower, M. A. Krutky, B.-S. Yang, and E. J. Perreault, "Use of self-selected postures to regulate multi-joint stiffness during unconstrained tasks," *PLoS One*, vol. 4, no. 5, pp. 1–11, May 2009.
[83] T. Flash, "The control of hand equilibrium trajectories in multi-joint arm movements," *Biol. Cybern.*, vol. 57, no. 4, pp. 257–274, 1987.
[84] J. Hermus, J. Doeringer, D. Sternad, and N. Hogan, "Separating neural influences from peripheral mechanics: The speed-curvature relation in mechanically constrained actions," *J. Neuriophysiol.*, vol. 123, no. 5, pp. 1870–1885, 2020.
[85] J. Hermus, D. Sternad, and N. Hogan, "Evidence for dynamic primitives in a constrained motion task," in *Proc. 8th IEEE RAS/EMBS Int. Conf. Biomed. Robot. Biomechatronics*, 2020, pp. 551–556.
[86] M. C. Nah, A. Krotov, M. Russo, D. Sternad, and N. Hogan, "Dynamic primitives facilitate manipulating a whip," in *Proc. 8th IEEE RAS/EMBS Int. Conf. Biomedical Robot. Biomechatronics (BioRob)*, 2020, pp. 685–691.
[87] J. A. Hoffer and S. Andreassen, "Regulation of soleus muscle stiffness in premammillary cats: Intrinsic and reflex components," *J. Neuriophysiol.*, vol. 45, no. 2, pp. 267–285, 1981.
[88] C. N. Maganaris, "Force-length characteristics of in vivo human skeletal muscle," *Acta Physiol. Scand.*, vol. 172, no. 4, pp. 279–285, Aug. 2001.
[89] V. Schettino *et al.*, "Geometrical interpretation and detection of multiple task conflicts using a coordinate invariant index," in *Proc. IEEE/RSJ Int. Conf. Intell. Robots Syst.*, 2020, pp. 6613–6618.

**James Hermus** received the B.S. degree in biomedical engineering from the University of Wisconsin-Madison, Madison, WI, USA, in 2016, and the M.S. degree in mechanical engineering from the Massachusetts Institute of Technology, Cambridge, MA, USA, in 2018. He is currently working toward the Ph.D. degree at the intersection of human motor control, robotics, and neuroscience.

His work investigates human physical interaction. He is especially interested in research that will aid individuals with disabilities.

**Johannes Lachner** received the skilled worker's certificate in mechatronics from the Chamber of Commerce and Industry (IHK), Bavaria, Germany, in 2012, the B.Eng. degree in mechatronics from University of Applied Sciences Augsburg, Augsburg, Bavaria, Germany, in 2013, the M.Eng. (Hons.) degree in mechatronic systems from the University of Ulster, Belfast, Ireland, and University of Applied Sciences Augsburg, in 2014. He is currently working toward the Ph.D. degree, supervised by Prof. Dr. Stefano Stramigioli (University of Twente, Enschede, The Netherlands) and Prof. Dr. Neville Hogan (MIT).

He joined KUKA, Augsburg, in 2014 and is currently a Senior Research Engineer at KUKA's corporate research department. He has published seven German, five European, and two international patents. His research interests include robot control with focus on physical human-robot interaction and mathematical description of robotic systems with differential geometric methods.

**David Verdi** received the B.S. degree in mechanical engineering from Columbia University, New York, NY, USA, in 2017, and the M.S. degree in mechanical engineering from the Massachusetts Institute of Technology (MIT), Cambridge, MA, USA, in 2019.

He is currently a Robotics and Control Systems Engineer (Systems Analyst) at Intuitive Surgical, Sunnyvale, CA, USA. His areas of interest have included compositional impedance control for accomplishing complex tasks and novel formulations of nullspace projection methods in robotics. In his professional capacity, he works on the design and control of minimally invasive surgical robots.

**Neville Hogan** (Member, IEEE) received the Diploma degree in engineering (with distinction) from the Dublin Institute of Technology, Dublin, Ireland, in 1970, and the M.S. and Ph.D. degrees in mechanical engineering from the Massachusetts Institute of Technology (MIT), Cambridge, MA, USA, in 1973 and 1977, respectively.

He joined MIT's faculty in 1979 and is currently Sun Jae Professor of Mechanical Engineering; a Professor of Brain and Cognitive Sciences; and directs the Newman Laboratory for Biomechanics and Human Rehabilitation. He cofounded Interactive Motion Technologies, now part of Bionik Laboratories. His research interests include robotics, motor neuroscience, and rehabilitation engineering, emphasizing the control of physical contact and dynamic interaction.

Dr. Hogan is a recipient of Honorary Doctorates from Delft University of Technology and Dublin Institute of Technology; the Silver Medal of the Royal Academy of Medicine in Ireland; the Saint Patrick's Day Medal from Science Foundation Ireland; the Henry M. Paynter Outstanding Investigator Award and the Rufus T. Oldenburger Medal from the Dynamic Systems and Control Division of the American Society of Mechanical Engineers; the Engineering in Medicine and Biology Society's Academic Career Achievement Award and the Robotics and Automation Society's Pioneer in Robotics Award, both from the IEEE.

Authorized licensed use limited to: MIT Libraries. Downloaded on February 09,2022 at 17:31:09 UTC from IEEE Xplore. Restrictions apply.